A SPECTROSCOPIC INVESTIGATION OF COMBUSTION-DRIVEN SPHERICAL IMPLOSION WAVES

by

D. E. Roberts

September, 1969. UTIAS Technical Note No.140

A SPECTROSCOPIC INVESTIGATION OF COMBUSTION-DRIVEN SPHERICAL IMPLOSION WAVES

by

D. E. Roberts

Manuscript received May, 1969.

September, 1969. UTIAS Technical Note No. 140

ACKNOWLEDGEMENT

I should like to thank Professor G. N. Patterson for providing the opportunity to work at the Institute for Aerospace Studies, and Professor I. I. Glass for suggesting this problem and supervising the investigation.

I should also like to thank my colleagues, particularly Messrs. W. C. Burgess, A. Elsenaar, W. O. Graf and Dr. A. K. Macpherson, for considerable assistance and helpful suggestions.

I am also indebted to Professor R. W. Nicholls for allowing me to use the facilities of the Spectroscopy Department, York University.

This research was funded by the Aerospace Research Laboratory of the U.S.A.F. under contract No. AF 33(615)-5313 and the National Research Council of Canada.

SUMMARY

A spectroscopic study has been made of imploding shock waves in a hemispherical chamber filled with an H_2-O_2-He mixture at high initial pressures (> 100 psi). In particular, temperature measurements at the origin of the chamber were made. Specific attention was paid to the use of the device as a driver for the UTIAS Implosion-Driven Hypervelocity Launcher.

The temperature at the origin, after an initially unreproducible phase corresponding to the explosion of a wire to detonate the mixture, remained constant at $\simeq$ 3000°K, virtually independent of the initial conditions. At the first implosion the temperature rose to typically 4000-5000°K for $\simeq$ 5μsec. later decaying rather rapidly.

The actual peak temperature reached was somewhat unreproducible and photographic observations showed this could be correlated with the degree of collapse at the origin. Calculations showed that heat conduction or radiation losses were completely unimportant in limiting the minimum size of the high-pressure, high-temperature region and this was clearly determined by the initial lack of symmetry of the converging shock waves. Neither does ablation appear to be an important limiting mechanism and even at the comparitively low measured temperatures the escape speed is ~ 60,000 ft/sec.

A semi-empirical study of the launcher performance, based on the observation that the behaviour followed that of a classical implosion, led to calculated velocities in reasonable agreement with microwave measurements of the velocity achieved during the first acceleration pulse. In particular, the performance was found to be not at all critically dependent on the degree of collapse near the origin.

Comparison with artificial viscosity technique calculations by other authors showed generally good agreement assuming an uncritical "limiting radius" cut-off was applied at the implosion to better reproduce the physical situation. This cut-off prohibited the ideal lossless calculated temperatures and pressures reaching extreme values near the origin by limiting the size of the high-pressure region to a finite value equal to that of the observed luminosity of this region.

TABLE OF CONTENTS

		PAGE
	NOTATION	
1.	INTRODUCTION	1
	1.1 Objectives of Launcher Programme	1
	1.2 Principle of Operation of Launcher	1
	1.3 Performance Calculations	1
	1.4 Performance Measurements	2
2.	OBJECTIVES OF SPECTROSCROPIC WORK	2
3.	EXPERIMENTAL EQUIPMENT	3
	3.1 The Launcher Chamber	3
	3.2 Ignition System	3
	3.3 Diagnostic Equipment	4
4.	CALIBRATION OF SPECTROMETER SYSTEM	4
	4.1 Wavelength Calibration	4
	4.2 Intensity Calibration of Photographic Plates	4
	4.3 Intensity Calibration of Photoelectric Detection System	5
5.	PRELIMINARY DIAGNOSTICS	5
	5.1 Time Integrated Spectra	5
	5.2 Time Resolved Photoelectric Recordings of Visible Radiation	6
	5.3 Intensity Records at Short Wavelengths	6
	5.4 Photography of the Implosion	7
	5.5 Comparison of Calculated Wave Trajectories with Measurements	7
6.	TIME RESOLVED TEMPERATURE MEASUREMENTS	8
	6.1 Shuttered Spectra	8
	6.2 Photoelectric Measurements of the Temperature	9
	6.3 Comparison of Measured and Calculated Temperature Histories	10
	6.4 Further Analysis of Preliminary Results	11
	6.5 Estimation of Heat Conduction and Radiation Losses	12
7.	CLASSICAL IMPLOSION CALCULATIONS OF LAUNCHER PERFORMANCE	14
8.	CONCLUSIONS	16
	REFERENCES	18
	APPENDICES	
	FIGURES	

NOTATION

B	Black body radiation function ; subscript referring to barrel
E	Exposure of plate
f	Projectile acceleration
i	Subscript referring to implosion
I	Intensity of radiation
k	Boltzmann constant
K	Thermal conductivity
m	Mass of projectile
N	Particle density (number per unit vol.)
N(OIII)	Particle density of doubly ionized oxygen
P	Pressure
Q	Artificial viscosity pressure
R	Shock radius
T	Transmission of photographic plate
t	Time
T	(Black body) temperature
V	Projectile velocity
W	Subscript referring to observation window
x	Co-ordinate of projectile down barrel
γ	Ratio of specific heats ; photographic constant
λ	Wavelength
σ	Stefan constant
δ	Classical implosion parameter

BLANK PAGE

1. INTRODUCTION

1.1 Objectives of the Launcher Programme

The UTIAS Implosion-Driven Hypervelocity Launcher conceived by Glass (see Ref.1) was designed to launch cylindrical projectiles of approximately 100 mg weight and 0.22" diameter (single calibre) by 0.22" long to hypervelocities (i.e. $\gtrsim$ 50,000 ft/sec). Projectiles with velocities of this magnitude are required for studies of meteoroid impact and satellite re-entry problems. The latter problem was of particular interest in which case it was desirable to have sufficiently large projectiles to hold some instrumentation and also to minimize distortion of the projectile under the very rapid launch acceleration ($\sim 10^8$ g's).

1.2 Principle of Operation of Launcher

The principle of operation of the UTIAS launcher can be understood with reference to Fig.1 (reproduced from Watson's report, Ref.2). The hemisphere is filled with a hydrogen-oxygen combustion mixture ($2H_2 + O_2$) at high pressure (typically 100-400 psi). This mixture could be diluted with helium or hydrogen. The gas is ignited by exploding a fine copper wire at the origin of the hemisphere creating a blast wave which decays into a steady detonation wave (Fig.1.1).

This hits the explosive liner (typically 0-200 grams PETN) the initiation of which generates a strong implosion (Fig.1.2). Subsequent reflection of this from the origin leaves a high-pressure, high-temperature region which drives the projectile down the barrel (Fig.1.4). The cycle is then repeated though without further input of energy. The device can be operated without an explosive liner, with a corresponding reduction of projectile performance.

In the following two sections we note some existing results of particular relevance to our study (i.e. mainly runs with zero explosive) but without comment at this stage.

1.3 Performance Calculations

All realistic calculations of the launcher performance have utilized the artificial viscosity technqiue, or "Q" method, of von Neumann and Richtmyer (Ref.3). In this method the usual shock relations for conservation of mass, momentum and energy are employed plus further energy terms to account for input of energy from the combustion zone and the explosive (if used).

An artificial pressure "Q" is included in the shock region to smear out the abrupt change in parameters across the shock or detonation front. The resulting smooth change in parameters is then calculated step by step by successive application of the shock relations with known boundary conditions to a series of zones across the shock. In the existing calculations "Q" is only employed for the purpose of ease of computation and has no relation to any real viscous effects. In fact, to date, the calculations are inviscid, non-heat-conducting and neglect radiation losses.

The first application of major relevance to the present work (i.e.

gas only runs) was made by Brode (Ref.4) who considered the imploding and reflecting waves in an enclosed chamber initially containing $2H_2 + O_2 + 7$ He at 100 psi. Because of the inviscid, lossless nature of the calculation the pressure and temperature diverged as the shock radius $R \to 0$. However, the calculations indicated ideal pressures $\sim 2 \times 10^4$ psi and temperatures $\sim 20{,}000^{\circ}K$ when R was $\leq$ the barrel radius. Such extreme conditions persisted for ≥ 5 μsec.

Flagg (Ref.5) used a semi-empirical, semi-analytical approach based on Brode's calculations to predict the launcher performance.

Sevray in parallel with Placest (see Ref.6) extended Brode's computational scheme to stoichiometric mixtures and to include the launching of projectiles and the effect of gas moving down the barrel. This work was further extended by Poinssot (Ref.7), who in particular used more zones in the calculation to give a better approximation to the inviscid shock structure.

More recently a detailed investigation of the utility of the "Q" method as applied to the launcher has been done by Elsenaar (Ref 8).

1.4 Performance Measurements

The first experimental study of the launcher using gaseous detonation waves without an explosive liner was made by Watson (Ref.2). His measured detonation velocities were in good agreement with the equilibrium Chapman-Jouguet calculations of Benoit (Ref.9). Pressure points on the reflection trajectories were also determined (before calculations noted in 1.3 were available). In addition Watson investigated the gun performance yielding terminal projectile velocities a factor of approximately 2x lower than subsequent calculations by Sevray (Ref.6).

Elsenaar (Ref.8) extended Watson's measurements to obtain detailed x-t histories of the projectile in the barrel by using the barrel as a resonant microwave cavity. The velocities measured after the first implosion were found in this case to be $\tilde{=}$ 2x higher than "Q" method calculations of Sevray, but in reasonable agreement with the revised calculations of Elsenaar.

Macpherson (Ref.10) has studied the detonation front photographically and found asymmetries amounting to typically $\tilde{=}$ 10% of the front radius.

2. OBJECTIVES OF SPECTROSCOPIC WORK

Before the present work the only direct measurements inside the chamber had been pressure recordings at two points along the top plate made by Watson (Ref.2). This was partly due to interest centering on overall performance (i.e. velocity measurements) and also due to the extreme conditions of temperature and pressure to which direct measuring instrumentation would be subjected e.g. on a 200 psi gas calculated (Ref.6) peak pressures after the first reflection amount to $\tilde{=}$ 2000 atmospheres.

The object of the spectroscopic work was therefore to measure basic parameters inside the launcher chamber, particularly temperature, which could be compared with existing calculations. Ideally such measurements could lead to an understanding of whether present measured and calculated velocity discrepancies are due to inherent limitations of the driver mechanism or other effects such as ablation (causing a lowering of the ideal escape speed) barrel

friction or leakage of gas around the projectile (leading to a counter pressure). In an ideal launcher it is desirable to have a high-temperature and low γ driver (Ref.1) and to maintain this high temperature for as long as possible during the acceleration phase of the projectile. It was intended to investigate these points spectroscopically and also the effect of variation of initial conditions (i.e., filling pressure, percentage dilution with helium) to determine empirically the optimum conditions for operation.

It was also important to know the degree of focussing of the converging shock waves and therefore photographic studies were undertaken to investigate this point. A study of the reflection of the imploding shock was particularly necessary since (as noted in 1.3) the calculated parameters diverge near the origin.

Pressure histories at the projectile base would also be of particular interest. However (for reasons discussed in Section 6.4) it was not possible in the present study to measure pressures spectroscopically.

One further problem of importance was that of projectile integrity currently being investigated by Graf (Ref.11). Clearly, time-resolved spectroscopy should enable some idea to be gained of the duration and magnitude of the acceleration pulses to which projectiles would be subjected and allow optimum conditions to be determined.

In the work described we concentrated particularly on the phase before the second reflection from the origin because Elsenaar's measurements (Ref.8) show typically $\simeq$ 70% of the peak velocity is reached between the first and second implosions. Calculations for the explosive case (Ref.6) show this phase is then even more important.

3. EXPERIMENTAL EQUIPMENT

3.1 The Launcher Chamber

The launcher chamber was an 8" diameter hemispherical cavity in a steel block (see Fig.2). The top plate containing the central observation port, the gas inlet and ignition electrode was secured by a steel nut. Pressure sealing was achieved by two sets of O-rings with brass backup rings. A more detailed description is given by Watson (Ref.2). The observation window was an expendable 1" diameter 1/4" thick quartz disc glued into a copper plug at the origin of the hemisphere (see Fig's. 2 and 4). When the device was operated as a gun the projectile would occupy this position. It was normal procedure to work with the chamber orientated such that the top plate was in a vertical position.

3.2 Ignition System

The gas mixture in the chamber ($2H_2 + O_2$ + He) was ignited by exploding a 2 mil copper wire of $\simeq$ 2 mm length at the origin ($\simeq$ 1 mm above the window surface). This explosion was driven by a 7.5 μfd, 6 KV capacitor switched by a thyratron (Ref.2). The wire current was only slightly damped with a first 1/2 period of about 10 μsec duration. The actual energy input to the exploding wire was about 25 joules (Ref.2) or about 0.01% of the gas energy at 200 psi.

3.3 Diagnostic Equipment

All spectroscopic observations were made with a Hilger medium quartz spectrograph. For photographic recording Kodak type 1-0 plates were used because of their high sensitivity (Ref.12). The correspondingly high granularity was found to be of little trouble in this work as most interest centered on continuum (black body) radiation.

Preliminary photoelectric recordings were made with a one channel spectrograph attachment (similar to the Hilger E720 unit) equipped with an RCA IP-28 photomultiplier with a type S11 sensitivity peaking at λ 3300Å. Later simultaneous measurements at 6 different wavelengths were rendered possible with a Hilger E751 "Strassheim" attachment. This unit mounted 6 EMI 6255B photomultipliers with a fairly uniform (type "S") sensitivity from λ 3000Å to λ 4200Å. Three of these photomultipliers covered the upper half of the exit spectrum and three the lower half. Each unit could be moved independently of the others. Three Keithly instruments type 246 power packs were used for the photomultiplier H.T.'s. Each output cable was matched to a 100 Ω resistor on one beam of a double beam scope (usually Tektronix type 555). The overall time response was normally $\tilde{}$ 0.2 μsec.

Time resolved photographs were taken with an S 11 visible response TRW framing camera (with 24B plug in unit) in conjunction with a 0 - 100 μsec variable delay unit.

4. CALIBRATION OF SPECTROMETER SYSTEM

4.1 Wavelength Calibration

When used for both photographic and photoelectric recording the wavelength calibration was performed using a low pressure helium lamp and a high pressure mercury lamp. Some of the stronger lines emitted by the latter were avoided because of their large broadening due to self absorption. The dispersions varied from 16.0Å/mm at λ3000Å to 69.0Å/mm at λ5000Å, covering most of the range of interest. Since line profiles were not of interest in this study higher dispersions were not necessary.

4.2 Intensity Calibration of Photographic Plates

Relative intensity calibration of the photographic plates was performed by developing in freshly prepared solutions of known strength at fixed temperature thereby characterising the γ of the plate (Ref.12). The exposure, E, was estimated from (Ref.12).

$$E = (1/T)^{1/\gamma} = (I_m/I_t)^{1/\gamma}$$

where T is the transmission of the plate at a particular λ. I_t is the transmitted intensity at λ and I_m the maximum transmitted intensity of the unexposed plate, both these quantities being measured with a microdensitometer. The incident intensity on the plate per unit wavelength interval was obtained (in arbitrary units) from the exposure by accounting for the variable dispersion of the instrument and the relative sensitivity of the plate as a function of wavelength (Ref.12). The latter quantity fell so rapidly above λ 4200Å that no quantitative evaluation was possible in that region. Below about typically

λ 3700Å in the results obtained the radiation energy was not high enough to produce more than a gross fog so only qualitative spectral features could be obtained in this region.

4.3 Intensity Calibration of Photoelectric Detection System

Each of the 6 photomultiplier + light pipe and slit systems of the "Strassheim" unit was calibrated using a tungsten ribbon lamp as a standard. With a voltage drop of 2.11V and passing a current of 10.150 absolute amps, this lamp emitted radiation with a colour temperature of 2034°K. (calibration of this lamp was done by the N.R.C. report no. APRO-229). This was again folded in with the instrument dispersion to obtain the relative intensity calibration.

5. PRELIMINARY DIAGNOSTICS

In order to understand the general characteristics of the "gas only" detonation runs several preliminary investigations were undertaken. The diagnostics used were time integrated photographic spectroscopy, time resolved photoelectric radiation measurements at a specific wavelength or band of wavelengths and time resolved photography. The experimental arrangement is shown in Fig's. 2 and 3. Unless otherwise stated all runs were under the standard initial filling pressure of 200 psi, $2H_2 + O_2$.

Generally each run resulted either in the observation window being shattered or in the case of a "well defined" implosion a hole $\tilde{}$ 1/4" diameter being punched through the window (Fig.4). In order to estimate the extent of the subsequent blast region time integrated photos were taken (Fig.5). Apparatus placed at more than twice the visible blast radius from the axis was found to be completely undamaged.

5.1 Time Integrated Spectra

Typical time integrated spectra are shown in Fig.6 (a) and (b). In the run corresponding to 6(b) the entrance slight height was larger than the image of the observation window on the entrance slit. The strong line radiation therefore came from the shock heated gas after this window was destroyed. Figure 6(a) shows more clearly the radiation from the "contained" interval. This is predominantly continuous with numerous absorption lines superimposed. The strong absorption band at λ 3064Å is due to OH. Some lines came from as high an ionization stage as O III.

A densitometer trace of the plate in Fig. 6(a) is shown in Fig.7. The linear region of the plate response was compared with the black body radiation function:

$$B(\lambda,T)d\lambda = \frac{2C_1}{\lambda^5} \frac{d\lambda}{(e^{C_2/\lambda T})-1} \qquad (1)$$

where $C_1 = 5.95 \times 10^{-6}$ erg $cm^2 sec^{-1} steradian^{-1}$

$C_2 = 1.4386$ cm degree K

This function is seen to fit well with the observed plate exposure yielding a best fit temperature,

$$T = 2.500^{\circ}K \pm 200^{\circ}K$$

To get further insight into what this temperature referred to time resolved measurements were necessary.

5.2 Time Resolved Photoelectric Recordings of Visible Radiation

To obtain some idea of the reproducibility of the device a series of runs were performed with a photomultiplier monitoring the visible radiation. Typical recordings were shown in Fig's. 8 and 9. The general picture is as follows:

Strong rather unreproducible emission occurs for ~ 20 μsec. after the wire is ignited (Fig.8). This falls steadily to an almost constant value in the next ~ 50 μsec. There is a further sharp peak in emission which can be identified with the first reflection. This peak is comparitively reproducible though sometimes structure is seen and the duration (the 1/2 width of the intensity pulse above the background) varies by as much as a factor of 2x. After the first implosion the emission is completely unreproducible (see Fig.8) though sometimes it is possible to identify up to 3 subsequent implosions (Fig.9(b)). Typically some 500-700 μsec after ignition the window is destroyed leading to another sharp increase in emission (Fig.9). The mean time to first implosion (averaged over 9 runs) was 76.7 ± 1 μsec. Subsequent implosions occurred at 161 ± 7 μsec, 241 ± 8 μsec and 324 ± 3 μsec. The mean duration of the first implosion light pulse was 4.1 ± 2.1 μsec.

5.3 Intensity Records at Short Wavelengths

A further series of runs was done at short wavelengths ($<\lambda 4000\text{Å}$) selecting a small wavelength range only (100Å). A typical recording is shown in Fig.10. The implosion is now much more clearly seen, as expected (i.e., the hotter implosion region emits more strongly at short wavelengths) and occurs at 75.3 ± 2.2 μsec (averaged over 5 runs) in good agreement with the previous value. The duration however is shorter: 1.9 ± 0.7 μsec. Again this is as expected. I.e., If the temperature at the origin rises monotonically to a maximum at the first implosion and subsequently falls monotonically the time between two points at a certain temperature is shorter the higher the temperature. Since the higher temperature is reflected by stronger radiation at short wavelength the intensity pulse will be of smaller duration at short wavelengths.

The 50 μsec region noted before now emits very weakly and on all shots it was possible to identify a feature corresponding to reflection of the outgoing detonation wave off the liner at 32.5 ± 4.7 μsec. The second lump on the exploding wire region may be due to a further increase in temperature during the second current cycle.

Clearly the total visible radiation emitted is dominated by the main part of the cycle and not the exploding wire or implosion regions due to the comparitively shorter times over which these emit strongly. The temperature (2,500°K) measured from the time integrated spectra (Fig.7) therefore refers

to an average "ambient" origin temperature away from the implosions. This temperature does not appear to vary strongly (i.e., more than the quoted error limits) since the total intensity (αT^4 for a black body emitter) does not (Fig.8).

5.4 Photography of the Implosion

In order to determine the degree of focussing of the first imploding shock wave a series of framing camera photographs were taken. These showed (e.g. Fig.11) an apparently stable implosion the resulting luminous region collapsing to about 0.6 cms diameter at the same time (76 μsec) as the previously measured values (see Fig.12). The typical duration of the collapse was also similar ($\simeq$ 4 μsec) to the previous values.

These measurements confirmed indirect observations using a copper "witness" plug at the origin which would be dented by a "well focussed" implosion (Ref.5).

5.5 Comparison of Calculated Wave Trajectories with Measurements

The calculated mean wave trajectories of Sevray (Ref.6) are shown in Fig.12 together with points taken from Poinssot's results (Ref.7). We took those points corresponding to the peak calculated pressure and their large spread is due partly to the fact that the "peak" of the shock is not well defined (particularly due to the computational "viscous" spreading of the shock zone) and partly because it is difficult to define an ingoing or outgoing wave near the origin. Generally, however, the mean trajectories are similar to Sevray's but correspond to higher velocities. The points determined spectroscopically (5.2 and 5.3) correspond to still higher velocities. It is clear that the number of zones used in the calculation (20 by Sevray, 56 by Poinssot) has quite a strong influence on the results. Note that the motion of the projectile down the barrel is generally rather small between the first and second implosions.

A more detailed study of the first cycle, including the points obtained from pressure recordings (Ref.2) is shown in Fig.13. The inter-correlation of the experimental results is good. The outgoing wave has a trajectory closely comparable with a Chapman-Jouguet detonation wave corresponding to the critical temperature and pressure (the calculated velocity of this wave was obtained from Ref.9). This is possibly somewhat fortuitous. Probably the wire after some delay explodes producing an overdriven wave with gradual decays to its equilibrium value.

The reflected wave speeds up after reflection from the liner, its velocity increasing as its radius decreases. The points have been fitted to a classical implosion trajectory (e.g. Ref.1) with the property

$$R = \text{const.}\ t^{\left(\frac{2}{2+\delta}\right)}$$

where, δ is a function of the specific heat ratio.

The best fit $\delta = 0.9 \pm 0.2$ is in fair agreement with the calculated δ of 0.67 (Ref.5) expected for a $\gamma \sim 1.2$. This γ would be consistent with the expected conditions of temperature and pressure behind the shock front (from Ref.8) and equilibrium property calculations (Ref.13).

6. TIME RESOLVED TEMPERATURE MEASUREMENTS

6.1 Shuttered Spectra

The preliminary measurements showed clearly that, at least at visible wavelengths the radiation emitted during the bulk of the wave cycle completely overwhelmed that emitted during the implosion. Therefore a shutter was built fulfilling the requirements of a transmission time ≃ 10 μsec. (i.e. 2x that of the observed duration of enhanced radiation - Section 5.2) which could be opened at any preset time after ignition.

A rotating disc shutter was used, the operation of which can be understood with reference to Fig.14. The laser beam pulse. detected via slit A, could be used to trigger the oscilloscope, the 20V gating pulse of this being used to trigger the ignition system after a predetermined delay. After a further delay determined by the shutter size, speed and θ (Fig.14 (b)) the shutter slit B becomes coincident with the spectrograph entrance slit. The delay between ignition and the shutter opening can be varied by adjustment of θ (Fig.15). The series of operations could be triggered manually by working on the single shot mode of the scope. Pressing the reset causes the next laser pulse to initiate the operation. Typical spectra taken with the shutter isolating the emission from the exploding wire and the first implosion phases respectively (initial pressure 300 psi, $2H_2 + O_2$) are shown in Fig's. 16(a) and (b). Figure 16 (a) shows that the strong radiation is still from a comparatively small region near the wire even after about 10-20 μsec from ignition. The implosion region (Fig.16(b)) taken for the same duration ≃ 70 μsec after ignition is clearly smaller than the window diameter (as in the framing photos Fig.11) and in this case off axis by about 3 mm.

Densitometer traces of Fig.16(a) and (b) are shown in Fig.17(a) and (b) respectively. The exploding wire emission shows strong molecular absorption features while the implosion region is completely continuous and is seen to fit well with a black body curve for T = 5,600°K ± 200. Conversely at such a low temperature (for particle densities as large as ~ 10^2 cm^{-3}) we expect the emission to be black body. This good fit and the lack of features indicitive of higher temperature, such as enhanced emission at short wavelengths or absorption lines suggest the temperature distribution does not differ strongly from a regular distribution. Studies of the first implosion for 100 psi and 200 psi mixtures yielded similar temperatures.

The main disadvantage in this method lay in the rather low plate exposures especially at short wavelengths where the strong wavelength dependence of relative intensities at different wavelengths could be used to advantage (i.e. from Eq.(1)).

$$\frac{B(\lambda_1,T)}{B(\lambda_2,T)} \alpha \left(\frac{\lambda_2}{\lambda_1}\right)^5 e^{(C_2/T)\left(\frac{1}{\lambda_2} - \frac{1}{\lambda_1}\right)}$$

At long wavelengths this ratio is independent of T

i.e.,

$$\frac{B(\lambda_1,T)}{B(\lambda_2,T)} \propto \left(\frac{\lambda_2}{\lambda_1}\right)^4 \quad (\text{for } C_2/\lambda T \ll 1)$$

The low observed exposure was consistent with the calculated energy incident on the photographic plate during the shutter open time and further measurements were therefore done with photoelectric detectors.

6.2 Photoelectric Measurements of the Temperature

The Hilger Strassheim attachment for the medium quartz enabled 6 wavelength regions to be monitored simultaneously (due to excessive noise on one channel only 5 were used in practice). The signals could be converted to relative intensities after correction for calibration (Section 5.2). The wavelength regions were chosen to be well away from any likely absorption or emission feature of the O_2-H_2 system. All measurements were interpreted in terms of black body emission except the rather irreproducible region up to ~ 20 μsec after ignition which was not of interest. Typical P-M recordings at three different helium dilutions are shown in Fig.18.

It should be noted that before this series of runs was done the chamber had to be remachined to 8-1/4" diameter following damage during an explosive run. Subsequent measurement showed longer times to implosion (c.f. Fig.13) than could be accounted for wholly on the basis of increased diameter. Also the focussing appeared to be poorer as evidenced by the inability of the luminous region, photographed with the S.T.L. camera, to collapse below the window diameter. On the other hand the gross performance of the launcher did not appear to be strongly affected. We discuss this further in Section 7.

The measured temperature at the origin versus time histories for several gas runs as a function of both initial pressure and dilution are shown in Fig.19. Also included for comparison are the earlier measurements described in Sections 5.1 and 6.1. We can make the following general comments about the results.

1) The temperature at the origin is virtually constant and of approximately the same value (2800-3500°K) independent of pressure for 45-50 μsec after the "exploding wire phase". Only at 400 psi is there a slight variation.

2) The temperature increases at the implosion but never by more than a factor of 2x the "ambient" value. The actual value reached is not reproducible and is clearly a function of the degree of focussing of the imploding shock. Framing camera shots corresponding to run 2(d) are shown in Fig. 21.(compared with Fig.11 which essentially corresponds to a run similar to 2(a)). Here there is no collapse below the window radius and the peak temperature is correspondingly much lower than in 1 (a).

3) There is no trend in peak temperature as a function of filling pressure within the limits set by reproducibility. The same is true of the effect of dilution of up to 40% of helium.

4) The times to implosion as a function of initial pressure and dilution show the trends expected (c.f. Ref's. 2 and 9) i.e., the higher the pressure and the higher the dilution with a high sound speed gas, the shorter the

time to implode. The "duration" of the implosion appears to follow the same trend.

6.3 Comparison of Measured and Calculated Temperature Histories

The paucity of calculations for our cases means we can only compare directly with the stoichiometric runs at 200 psi and 400 psi (calculations from Ref's. 6, 7 and 8) and draw general conclusions from the other results.

Firstly we note that due to the limited number of zones in the origin region the "Q" method calculations cannot be expected to be realistic in this region. Ideally one would have to use an increasing number of zones to describe the problem as one approached the origin and because the calculations are inviscid and lossless the results would gradually diverge (as in Brode's calculations for the $2H_2 + O_2 + 7$ He case described in detail by Flagg, Ref.5). This is illustrated in Fig.20 where maximum temperatures at the origin as calculations in Ref's. 7 and 8 are shown, the latter using an increased number of zones.

Since the minimum radius of the implosion front is clearly finite it seems reasonable to limit the calculation at this radius. One could then assume conditions do not vary in this radius and see how critical its value is on the predicted temperatures. This radius should obviously be of the same order as the "optical radius" (~6 mm) (section 5.4). The results of applying this procedure to the calculations are shown in Fig.22. Note that in the original calculations T was obtained from the ideal gas law PV = RT and therefore the equilibrium H_2-O_2 system calculations of Benoit (Ref.13) had to be used to apply a reiterative correction for dissociation etc.

We see that the final calculated temperatures at the origin are not critically dependent on the "cut off" radius and taking this to be the framing camera value or the window diameter depending on the degree of collapse, gives quite good agreement between measurement and computations (Ref.8). Well before the implosion the agreement is good independent of the zoning procedure.

There are two regions in which the agreement is poor. Firstly the initial 20 μsec is clearly very badly reproduced in the calculations where a Chapman-Jouguet detonation wave is set up immediately after ignition. Secondly, the measured temperatures fall off much more rapidly after the implosion.

The shape of the calculated temperature profile is quite dependent on the pressure, via the correction of the ideal gas temperatures, since this correction is a function of the molecular weight. The slower fall off in T could therefore in part be due to a faster fall off in pressure.

These apparently low peak temperatures are actually physically quite reasonable. The first implosion wave moves into a preheated gas (from the detonation wave) and even ~ 4 mm from the origin still has a Mach number of $\lesssim 3$. It is only very near the origin (< 1 mm) that the shock is sufficiently strong to give temperatures > 10,000°K. As we have seen, such a high degree of collapse does not occur.

It is of interest to compare our temperature measurements with those obtained on two completely different devices. These devices have, however,

the common feature of a gas being shock heated such that, in the lossless limit, an infinite discontinuity is obtained, i.e., P, T $\rightarrow \infty$ when same scale length (c.f.R) tends to zero.

In the first of these devices (Belokon' et al, Ref.16) a shock wave travels down a wedge cavity and is reflected at the apex. The peak measured temperatures at this apex (which ideally $\rightarrow \infty$) were $\simeq$ 40,000°K. Our results can be considered as consistant with these in that the temperature is limited to comparitively low finite values. Their higher values can be explained both on the basis of the smaller "collapse" region (i.e. 0.5 - 1 mm) and the far lower pressures ($\simeq$ 0.1 torr). In fact these authors found the temperature decreased considerably as the initial pressure was increased (T = 43,000°K for P_i = 0.1 torr' T = 33,000°K for P_i = 0.2 torr).

Knystantas et al (Ref.17) measured the temperature at the origin of a cylindrical imploding detonation wave in gas mixtures at initial pressures from 50 to 120 torr. They claim a peak T $\sim$ 189,000°K. However, their use of Wien's law (i.e, Eq. (1) with the 1 in the denominator neglected) is completely invalid since for the conditions they quote $e^{C_2/\lambda T} \sim 1$. The actual temperature consistent with their results is certainly far lower than the quoted figure.

6.4 Further Analysis of the Preliminary Results

In view of the results recorded in 6.2 it is of interest to view the preliminary results in retrospect. Firstly we can attempt to infer the temperature at the implosion, T_i, from the measured "ambient" temperature, $T_a \simeq$ 2,500°K. Thus at λ 3656Å (see Fig.10) the ratio of the implosion intensity to that $\sim$ 20 µsec earlier is 28. At λ 3961Å this ratio was found to be 17. This is consistent with an increase in temperature (for black body radiation) of a factor of 1.92 giving T_i = 4,800°K in good agreement with the "well focussed" measurements.

If we now consider the absolute intensities corresponding to T_a and T_i.

$$\frac{I(T_i)}{I(T_a)} = \frac{T_i^4 r_i^2}{T_a^4 r_w^2} \simeq 2.5$$

where

$I = \sigma T^4 = 5.67 \times 10^{-12} T^4$ watts/unit area

r_i is the implosion radius

r_w is the window radius

The observed ratio in the visible agrees well with this figure implying that the first implosion does not strongly impair the transmission of the window. This view is confirmed in the more recent runs (6.2) where now $r_i \geq r_w$ and also less direct evidence was given by highly diluted runs ($2H_2 + O_2 + 7He$) where no detonation wave was formed and the window was not destroyed. Subsequent examination of the window showed deposits of copper from the exploding wire but the transmission was diminished by < 5% and the

relative transmission at different wavelengths essentially unchanged.

If we calculate the total intensity as a function of time using reasonable shapes for the temperature and emitting area as functions of time (Fig.23 (a) and (b)) we find a dip corresponding to the implosion (Fig. 19 (c)) in good agreement with observation (e.g. Fig.8 (b)). It therefore appears that the structure on the observed light pulse was not due to structure in the reflected imploding wave but a direct reflection of collapse below the window diameter. The later recordings (6.2) often showed no structure in agreement with the observation of no collapse below the window radius (Fig.21).

Finally we note that it is not possible to estimate pressures from emitted intensities studies. Ideally absorption line shapes could be used to obtain population densities corresponding to the lower states of the lines observed. Knowing the temperature, all other relevant population densities and then the pressure could be obtained by assuming local thermodynamic equilibrium. This would be a very good assumption for the large particle densities ($\sim 10^{21} cm^{-3}$) at the implosion. For some of the high calculated temperatures (10^5-$10^6{}^oK$) attained in explosive runs (Ref.1) the gas could be optically thin in the near ultra violet and it is possible that lines could be used for the above purpose. However, at the low measured temperatures for gas runs no structure could be expected.

6.5 Estimation of Losses Due to Radiation and Heat Conduction

(a) Radiation Losses

Knowing the temperature and quality of the emitted radiation it is now possible to make reasonable estimates of losses. If we assume at the implosion all the radiation emitted is lost from the surface of a hemisphere of the size measured photographically the ratio of energy lost to thermal energy contained in the implosion is:

$$R = \frac{\sigma T^4 \, 3\pi r_i^2 t}{N k T (2/3) \pi r_i^3}$$

where N is the particle density. The initial particle density (at 200 psi) = 3.66×10^{20}. This will be increased by a factor C at the implosion; t is the duration of the implosion $\simeq$ 5 μsec.

$T \sim 5{,}000^oK \qquad r_i \simeq 0.25$ cms

giving $R = \frac{1.15 \times 10^{-3}}{C}$

typically the calculated C$\sim$ 5 giving R $\sim 0.58 \times 10^{-3}$/

R scales as T^3/r and is = 1 for $T \simeq 60{,}000^oK$.

At higher temperatures the radiation will be less than that emitted by a black body at short wavelengths. If we take a typical figure for the peak temperature and pressure calculated for an explosive run i.e., $10^{6o}K$ and 10^6 psi respectively we find via a reiterative calculation the equilibrium composition

as follows: $n_e = 38.10^{20}$, n(OVI) = 3.3×10^{16}, n(OVII) = 4.8×10^{19}, n(HII)= 9.5×10^{19}). The total continuum emission (free-free+free bound) (limited by the black body limit where this is smaller) is found to be ~ 10^{12} watts/cc.

We then find R ~ 10^3 (independent of C).

It is therefore clear that radiation losses completely prohibit the attainment of the inviscid-lossless calculated temperatures for times as long as ~ 5 μsec. Similar conclusions also hold for peak T = 10^{5}°K, peak P= 10^5 psi.

(b) Heat Conduction

The conductivity, K, is given by (Spitzer, Ref.14)

$$K = \frac{k\bar{V}}{2\sigma}$$

A typical molecular velocity (OH at 5,000°K) is V = 1.6×10^5 cms sec^{-1}.

Using a radius = 10^{-8} cms the relevant cross section $\sigma \simeq \pi \times 10^{-16}$ cm^2, giving K = 0.35×10^5 c.g.s. units.

Assuming a reasonable temperature gradient of,

$$\frac{dT}{dx} = 0.5 \times 10^{4} \text{°K/cm}$$

the heat flux in t = 5 μsec, assuming no contact with the walls at the implosion is,

$$\phi = \frac{-K\, dT}{dx}\, t = 0.83 \times 10^3 \text{ ergs}$$

Compared with the energy content NkT x $(2/3)\pi r_i^3 = 4.2 \times 10^7$ ergs, ϕ is clearly negligible the ratio, R', being 2×10^{-5}, R' scales approximately as $(1/T^{1/2})(dT/dx)$ and even for peak temperatures = 10^{6}°K could still be $\ll 1$ assuming not too severe temperature gradients.

To summarize, therefore, neither radiation losses nor heat conduction appear to limit the temperature obtained at the implosion during gas runs. Improvements in the artificial viscosity calculations in this direction are not therefore worthwhile.

It seems most likely that the finite size of the implosion region and comparitively low peak temperatures are a result of non ideal symmetry of the converging shock waves. This lack of symmetry is indicated by the large spread (~ 4 μsec) in the times to reach the liner (see 5.3) from ignition compared with the small uncertainty in implosion times (1 μsec) and more directly by Macpherson's (Ref.10) photographic evidence.

With respect to the explosive driver runs radiation losses would certainly prohibit the attainment of temperatures anywhere near 10^{5}°K for even as long as 1 μsec. However, as for the gas runs, the limiting factor of the ultimate size and temperature and pressure would certainly again be lack of absolute symmetry of the implosion. (Note added in proof: Very recent work

has shown that nearly ideal focussed implosions can be produced using $2H_2 + O_2$ only, as well as with explosive PETN).

It is clear that any technique which does not include the effects of asymmetry or instability (Ref.15) in the converging shock cannot give a true physical picture of conditions obtained near the origin at the implosion. On the other hand, the calculated force on a projectile near the origin may not be critically dependent on the details of the implosion behaviour. In order to obtain some insight into this, simple velocity calculations were performed as described in the following section.

7. CLASSICAL IMPLOSION CALCULATIONS OF LAUNCHER PERFORMANCE

It is of interest to know what implications the previous results have on the limitations of or predictions that can be made about the overall launcher performance i.e., projectile velocity. The performance was therefore calculated using a classical implosion model which we shall now discuss.

Firstly we note that a classical implosion, $R = \text{const}\ t^{2/(2+\delta)}$ with $\delta = 0.9 \pm 0.2$ gives a good fit to the measured trajectory. It is therefore reasonable to assume that the peak pressure behind the shock, P_m, is also given by the classical relation, $P_m = \text{constant}\ R^{\delta}$, with the same δ. It seems likely that this will not be a good description of the actual pressure history both near the wall and the origin e.g., in particular, we might expect δ, which is a function of γ, to vary. However we can fix the constant by anchoring this relation to a "well defined" pressure somewhere in the middle of its trajectory and see whether the limiting regions, the wall and the origin are critical on the results.

We now make two further assumptions, that the reflected pressure history is the same as the incident history and that the pressure across the reflected shock is the classical value 3.33, for $\delta = 1.4$ (Ref. 1).

Finally we have to assume a form for the fall off of pressure behind the shock. Initially we assume no fall off and later find out how critical is the chosen fall off.

If the radius of the reflected implosion wave $R < R_B$, the barrel radius, we assume there is a uniform pressure over the area πR^2 and zero pressure outside. Clearly the criticality of this assumption also has to be checked. For $R > R_B$ the driving area is constant $= \pi R_B^2$.

We then find (see Appendix I for details)

For $t \leq t_B$ $$\frac{V(t)}{V_s} = 3.33 \left(\frac{2+\delta}{6-\delta}\right) \left(\frac{t}{t_s}\right)^{\frac{6-\delta}{2+\delta}}$$

For $t > t_B$ $$\frac{V(t)}{V_s} = \frac{V(t_B)}{V_s} + 3.33 \left(\frac{R_B}{R_s}\right)^2 \left(\frac{2+\delta}{6-\delta}\right) \left\{ \left(\frac{t}{t_s}\right)^{\frac{2-\delta}{2+\delta}} - \left(\frac{R_B}{R_s}\right)^{\frac{2-\delta}{2}} \right\}$$

where t_s is the time for the wave to reach the chamber surface radius, R_s,

after reflection at t = 0 and t_B is the time to reach the barrel radius, R_B, after reflection.

$$V_s = \frac{gP(R_s)\pi R_s^2 t_s}{m}$$

For convenience of notation the pressure has been normalized to that at the surface of the chamber. Instead of using $P(R_s)$ it is better to use the minimum value away from the surface where the "classical" variation of P might be particularly suspect.

If we consider the initial conditions 200 psi, $2H_2 + O_2$ a 0.67 gram projectile and 5/16" barrel for which the projectile x - t history has been measured (Ref.8) the effective $P(R_s) \sim 70$ bars.

The corresponding acceleration and velocity histories of the projectile are shown in Fig.24. For $\delta = 1$, $V \rightarrow$ const x $t^{1/3}$ at large t. For $t > 42$ μsec the wave should be reflected from the chamber surface and the acceleration increase again. However the projectile has now moved well away from the origin (cf. Fig.12) and the simple "enclosed" model used cannot be expected to hold well for such large times. The measured velocity for $t = 42$ μsec is seen to be about 40% higher than the calculated value (for $\delta = 1.0$). The choice of δ is seen to be not critical on the final ($t = 42$ μsec) velocity, a 20% change in δ causing about the same change in V.

In order to understand why the calculated velocity is too low we note one particularly bad feature of this model. That is the time during which the reflected imploding wave remains within the barrel diameter is clearly much less than the experimental values.

I.E. $t_B = 0.324$ μsec ($\delta = 1$)

$t_B = 0.45$ μsec ($\delta = 0.8$)

$t_B = 5$ μsec (experimental section)

The last time is really the "duration" of the high temperature region which is what is relevant here. This "slower than classical" behaviour is at least partly why the time between first and second implosions is greater than 76 μsec by $\simeq$ 5 μsec (Fig.12). If we now assume the classical behaviour still holds for $R > R_B$ but for $R < R_B$ the R - t behaviour is linear with a duration of 5 μsec. we then obtain (Appendix I) the acceleration pulse (b) and corresponding velocity profiles (b) which are in much better accord with experiment.

If we instead assume there is no collapse to a smaller radius than R_B but that the pressure remains essentially constant we obtain a further increase in final velocity of $\simeq$ 50%.

Since the minimum radius is typically $\simeq$ 0.3 cms (cf. $R_B = 0.4$ cms) the most realistic model would lie somewhere between (b) and (c) and would predict a velocity in quite good agreement with experiment.

We may therefore draw the following general conclusions:

(a) The acceleration during the time for which $R_s > R > R_B$ accounts for about half the projectiles final velocity. The result is not at all critically dependent on the model used, in particular the choice of δ or the fall off of pressure behind the front.

(b) During the time for which $R < R_B$ the projectile is accelerated to typically half its final velocity. The "duration" of the implosion must be included empirically in the calculation and affects linearly the velocity attained by the time $R = R_B$. However a change of 50% in t_B only affects the final calculated velocity by about 20%.

If one assumes no collapse for $R < R_B$ then a 50% higher velocity is obtained compared with the assumption of a collapse to $R = 0$. This implies that within limits it is detrimental to the performance to have a high degree of focussing (assuming the wave is still centered) because the increase of pressure at the origin is more than compensated by the decrease of effective area over which this is applied. The optimum final radius on this picture would be $R = R_B$.

It does not appear likely that the behaviour near the barrel radius can be better treated by the "Q" method since the final radius is clearly limited by initial asymmetry of the imploding shocks whereas the "Q" method would give a divergent pressure near the origin and a similar acceleration profile to (a) though with a more realistic time for t_B.

The conclusion that good focussing is relatively unimportant tends to be supported indirectly by experiment in that runs at the same initial pressure but taken at quite different times tend to yield no significant differences (i.e., more than ≃ 15%) in projectile velocity (see Ref.8). It seems highly likely that the focussing was not reproducible throughout these runs (c.f. Section 6.4). A possible alternative explanation is that an initially well focussed implosion might give a somewhat smaller velocity for the first cycle than the optimum case. However the subsequent implosion may lead towards the optimum case giving a larger increase in velocity than the second case. Generally speaking therefore differences in implosions might be expected to be "evened" out as far as the final actual velocity is concerned.

8. CONCLUSIONS

We have shown that the peak temperature attained at the origin for a gas-driven implosion is limited to comparitively low values (4000-5000°K) most probably due to non-ideal symmetry of the converging shock waves. Contrary to earlier suggestions neither radiation, conduction, or ablation losses appear to be at all important. That the implosion front is not grossly unstable can be understood from the suggestion of Ahlbom and Huni (Ref.18). A perturbation of radius of curvature, less than that of the main front would move faster than the main front and would therefore tend to catch up with it.

In fact the low temperature does not appear to be a serious limitation of the driver properties. The escape speed is still high (≃ 60,000 ft/sec). Also, because an increase of temperature and pressure at the origin is accompanied by a corresponding decrease of area over which the pressure is effective, the force on the projectile is not strongly affected by changes in conditions at the

implosion. In addition, it seems possible that first implosions with different degrees of convergence tend to compensate on successive implosions leading to similar final velocities.

It does not therefore seem worthwhile expending effort in attaining a high degree of collapse at the origin. Indeed it is possible that this might be slightly detrimental to the performance owing to the very high local peak pressures. The optimum situation possibly being where the final collapse radius ~ the barrel radius. Even if a high degree of symmetry of the converging shock waves were attained, it seems likely that inherent instability would strongly limit the conditions at the origin (Ref.15). Lastly, radiative losses anyway prohibit the attainment of temperatures as high as 60,000°K.

Semi-empirical "classical implosion" calculations of the velocity after the first cycle give quite good agreement with experiment. More detailed artificial viscosity calculations by Elsenaar also gave good agreement and suggested the lower calculated velocities earlier were due to insufficient "zoning" near the origin. The agreement with the temperature measurements was also good assuming the final zone had a radius equal to the collapse radius. The fact that the final barrel velocities were higher than experiment in the earlier calculations therefore appears due to overestimation of the effects of subsequent cycles probably due to incorrect treatment of motion of gas down the barrel and assumption of an infinite escape speed. It seems likely that better treatment of these by Elsenaar can remove this discrepancy.

Generally speaking, therefore, experiment and computations agree quite well for the gas runs (see Sec.6.3). The measured velocities seem to be what one can expect (at least after the 1st cycle) and not strongly affected by any one parameter. This is indicated by the experimental results for the muzzle velocity, which show quite a small spread (~ 10%) in spite of what must have been quite a large variety of conditions (i.e., ignition arrangement, degree of focussing of shock waves, barrel friction, leakage of gas around the projectile).

For the explosive runs we have no spectroscopic data and can only draw on the above conclusions. Firstly, the ultimate process limiting the conditions at the origin is undoubtedly the same as in the gas case. i.e., lack of absolute symmetry of the imploding shock. Again temperatures as high as the ideal calculated values of 10^{5}°K - 10^{6}°K may be completely prohibited on the basis of radiation losses alone. Higher temperatures than in the gas case should be obtained but < 50,000°K due to losses. This may not lead to a larger escape speed, at least with the stoichiometric mixture, because the increased sound speed is balanced by an increased γ. In any case, the calculations show that even at temperatures ~ 50,000°K were attained it would only be over an area ~ 1 mm diameter. The "average" temperature over the projectile base would be much less.

At present velocity measurements for the explosive runs are typically 2x lower than existing calculations. The reasons for this disagreement are presently being further investigated in some detail.

REFERENCES

1. Glass, I. I. — Research Frontiers at Hypervelocities, Can. Aero. & Space Jl, 13, nos. 8 and 9, p. 347, 1967.

2. Watson, J. D. — Implosion Driven Hypervelocity Launcher Performance Using Gaseous Detonation Waves, UTIAS Tech. Note. No. 113, 1967.

3. von Neumann, J. Richtmyer, R. D. — A Method for the Numerical Calculation of Hydrodynamic Shocks, Jl. Appl. Phys. 21, 1955.

4. Brode, H. L. — Private communication: see Ref's. 2 and 5. Also see Ref.1. for other relevant references.

5. Flagg, R. F. — The Application of Implosion Wave Dynamics to a Hypervelocity Launcher, UTIAS Report No. 125, 1967.

6. Sevray, P.A.L. — Performance Analysis of UTIAS Implosion Driven Hypervelocity Launcher, UTIAS Tech. Note No. 121, 1968.

7. Poinssot, J. C. — A Preliminary Investigation of a UTIAS Implosion-Driven Shock Tube, UTIAS Tech. Note No. 136, 1969.

8. Elsenaar, A. — Microwave Measurements of Projectile Motion in the Barrel of the UTIAS Implosion-Driven Hypervelocity Launcher, UTIAS Tech. Note (to be published)

9. Benoit, A. — Properties of Chapman-Jouguet Detonations in Stoichiometric Mixtures of Hydrogen-Oxygen Diluted with Helium and Hydrogen, UTIAS Tech. Note No. 113, 1967.

10. Macpherson, A. K. — Work in progress.

11. Graf, W. O. — A Study of Projectile Integrity Under Extreme Conditions in a Hypervelocity Launcher, UTIAS Ph.D. Thesis (in progress)

12. — Kodak Plates and Films for Science and Industry, Eastman Kodak Co., 1962.

13. Benoit, A. — Equilibrium Thermodynamic Data for the H_2-O_2-He System, UTIAS Tech. Note No. 128, 1968.

14. Spitzer, L. — Introduction to the Physics of Ionized Gases, Interscience Pub. New York, 1956.

15. Zababakhin, E. I. — "Cumulation of Energy and its Limits", Soviet Physics USPEKHI, 8, no.2, p.295, 1965.

16. Belokon', V.A. Petrukhin, A. I. Proskuryakov, A.V. — "Entrance of a Strong Shock Wave into a Wedge-Like Cavity". Soviet Physics JETP, 21, no.1, p.33, 1965.

17. Knystautas, R.
Lee, B. H. K.
Lee, J. H. S.

"Diagnostic Experiments on Converging Detonations". 6th, Int. Shock Tube Symposium, Freiburg, Germany. 1967.

18. Ahlborn, B.
Huni, J. B.

A.I.A.A. Journal, to be published

APPENDIX I: LAUNCHER PERFORMANCE BASED ON A CLASSICAL IMPLOSION

A. We assume the peak pressure behind the ingoing shock wave has the classical behaviour,

$$P_m(R) = \text{const}\ R^{-\delta}$$

that is,

$$P_m(R) = P_m(P_s)\left({}^{R_s}/_{R}\right)^{\delta}$$

For a pressure increase k on reflection the pressure behind the reflected wave is

$$P_{m_R}(R) = k\ P_m(R_s)\left({}^{R_s}/_{R}\right)^{\delta}$$

For $t \leq t_B$ (corresponding to $R \leq R_B$) the force on the projectile is

$$F \simeq \pi R^2\ P_m(R_s)\left({}^{R_s}/_{R}\right)^{\delta}$$

assuming the fall-off in pressure behind the front is small. If we use the classical relation $R = \text{const}\ t^{2/\delta + 2}$ we get

$$V(t \leq t_b) = \int_o^t F/m\ dt = V_s\, k\left(\frac{2+\delta}{6-\delta}\right)\left({}^{t}/_{t_s}\right)^{\frac{6-\delta}{2-\delta}}$$

where,

$$V_s = \frac{g\ P(R_s)\ \pi R_s^2\ t_s}{m}$$

For $t \geq t_B$ we assume the pressure behind the front falls off from its peak value as $R^{-\delta}$. The pressure at R_B for $R > R_B$ is therefore,

$$P_{mR} = k\ P_m(R_s)\left({}^{R_s}/_{R}\right)^{\delta}\left(\frac{R_B}{R}\right)^{\delta}$$

The effective area over which this accelerates the projectile is now fixed = πR_B^2

$$V(t > t_B) = V(t_B) + kV_s\left(\frac{R_B}{R_s}\right)^2\left(\frac{2+\delta}{6-\delta}\right)\left[\left(\frac{t}{t_s}\right)^{\frac{2-\delta}{2-\delta}} - \left(\frac{R_B}{R_s}\right)^2\right]$$

APPENDIX I :

B. If instead we assume for $R \leq R_B$ that P_m = const R and R = const t with t_B = the experiment "duration" of the implosion ≈ 5 μsec and, as before, $P_{mR}(R_B) = P_m(R_s)\,(R_s/R_B)^{\delta}$ then

$$F\ (t \leq t_B) = \pi \frac{R^2\ g\ k}{}\ P_m(R_s)\,(R_s/R_B)^{\delta}\ \ R/R_B$$

and

$$V\ (t \leq t_B) = \pi \frac{R^2\ g\ k}{m}\ P_m(R_s)\ t^2/2t_B$$

$V(t \geq t_B)$ is given by the same expression as before.

In both cases for $t \gg t_B$ $\quad V(t) \rightarrow$ const $t^{\left(\frac{2-\delta}{2+\delta}\right)}$

$\approx$ const $t^{1/3}$

(using the measured $\delta \sim 1$)

This slow increase in V is quite consistent with experiment (Fig.25).

BLANK PAGE

1. OUTGOING DETONATION WAVE

2. DETONATION WAVE REFLECTS AS SHOCK WAVE (INITIATES LINER, IF USED)

3. MAIN SHOCK CONVERGES ON ORIGIN, BECOMING VERY STRONG

4. SHOCK WAVE REFLECTS ON ORIGIN AND MOVES OUT AGAIN

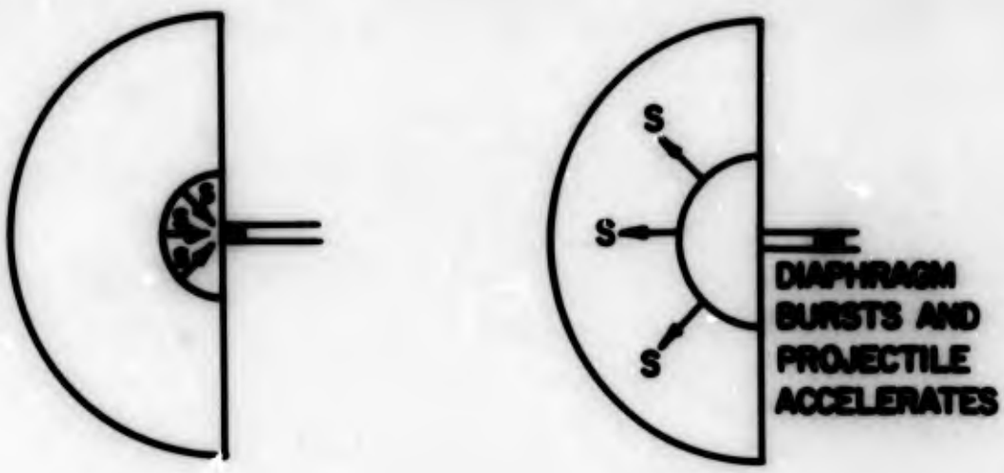

FIG. 1 SCHEMATIC OF IMPLOSION CHAMBER WAVE DYNAMICS (REPRODUCED FROM REF. 1)

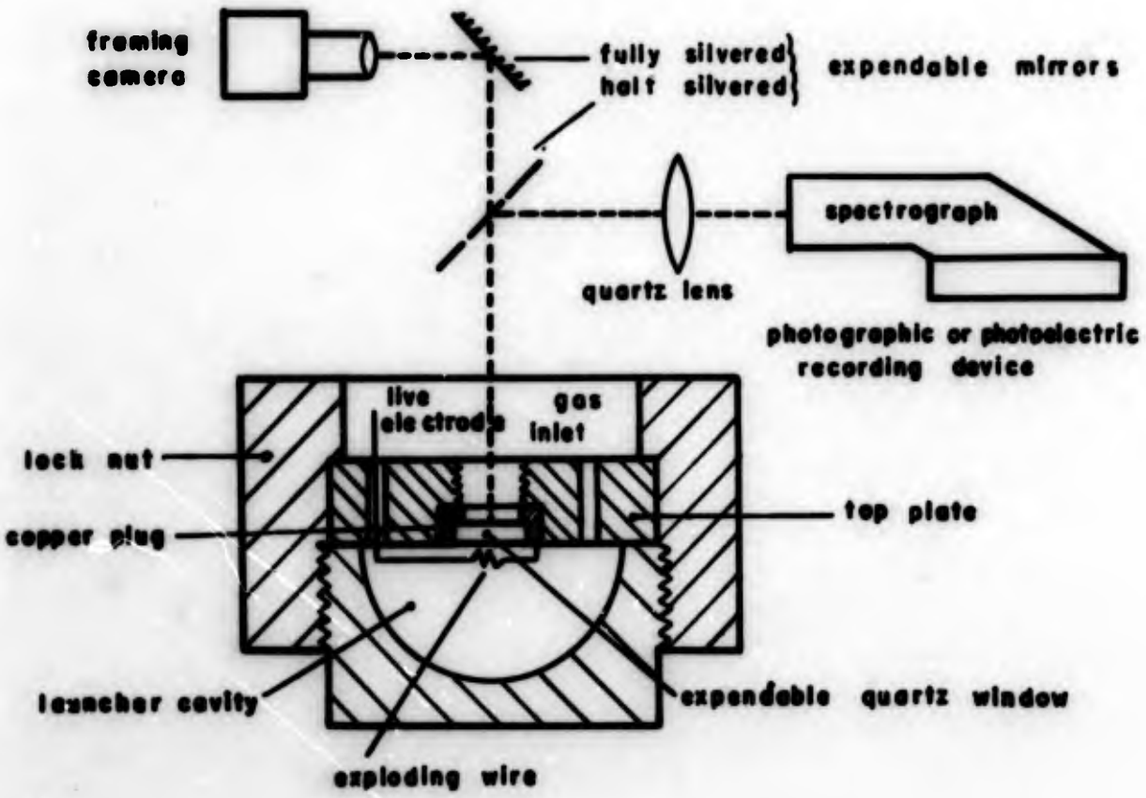

(a) GENERAL ARRANGEMENT (PLANVIEW).

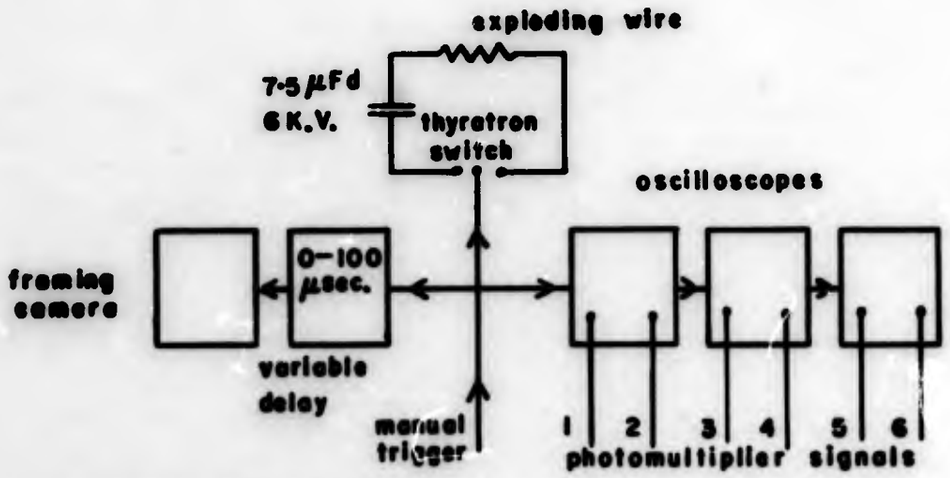

(b) SWITCHING PROCEDURE

FIG. 2 DIAGNOSTIC ARRANGEMENT.

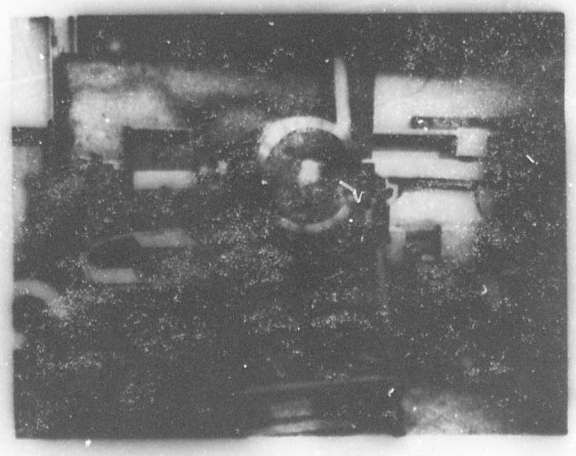

FIG. 3.

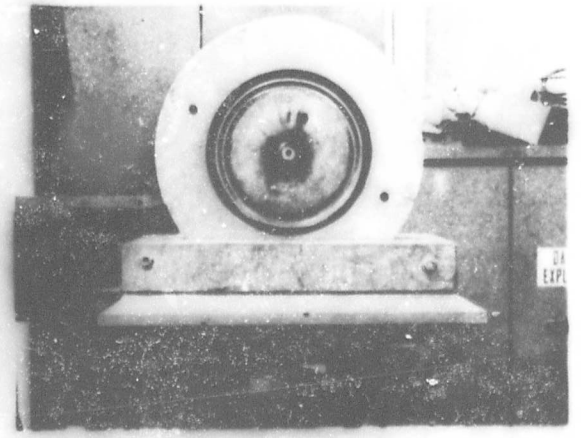

FIG. 4.

FIG. 5.

FIG.3: Rear view of launcher and diagnostic equipment. (See fig.2).

FIG.4: Top plate after a well defined implosion.

FIG.5: Time integrated photo of window blowing out.
(Same run as in fig.4).

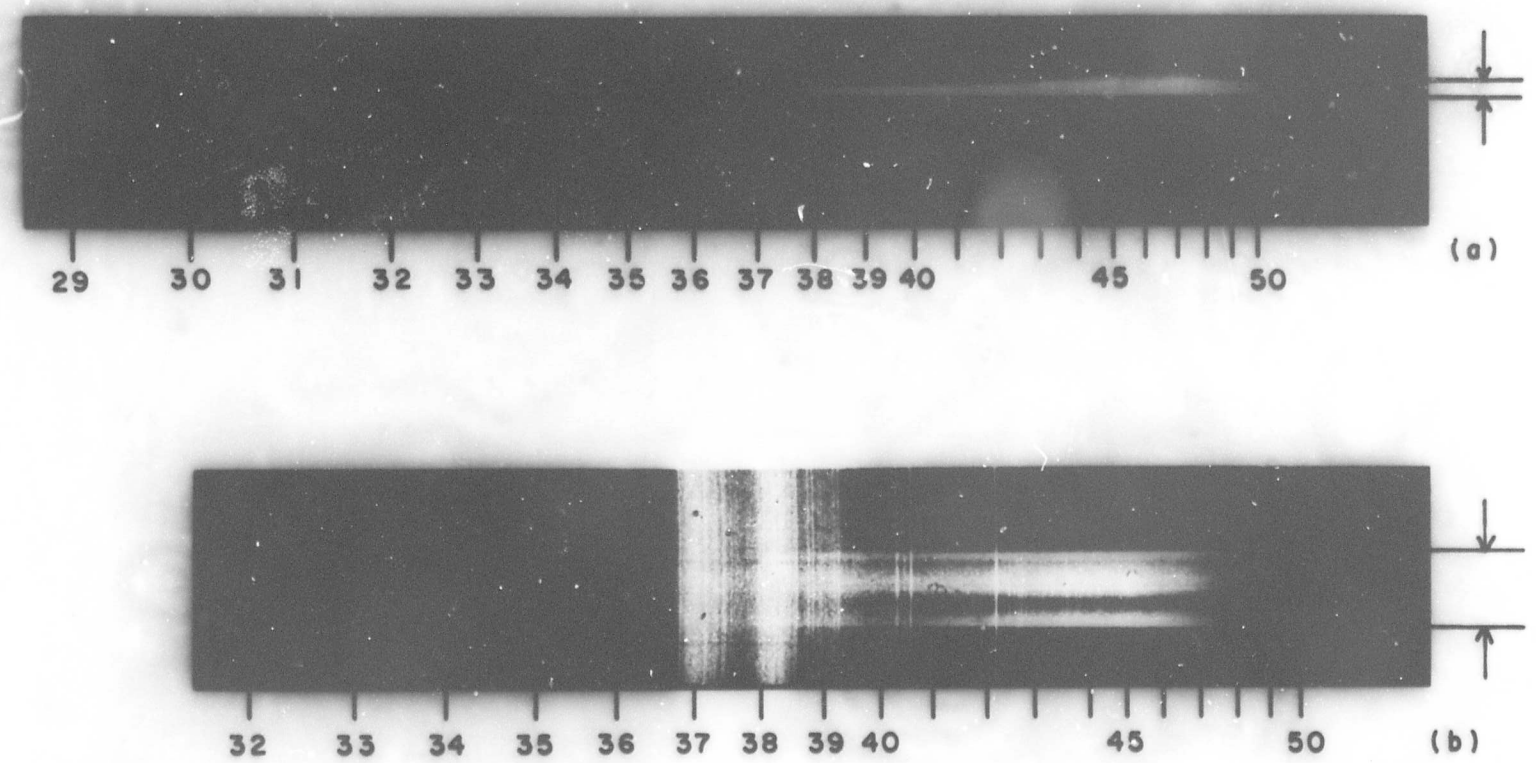

FIG. 6: TIME INTEGRATED SPECTRA OF TWO GAS RUNS [200 p.s.i., $2H_2 + O_2$].
(wavelength scale units of 100 Å).
(↓ / ↑ corresponds to size of image of 1/2" window).

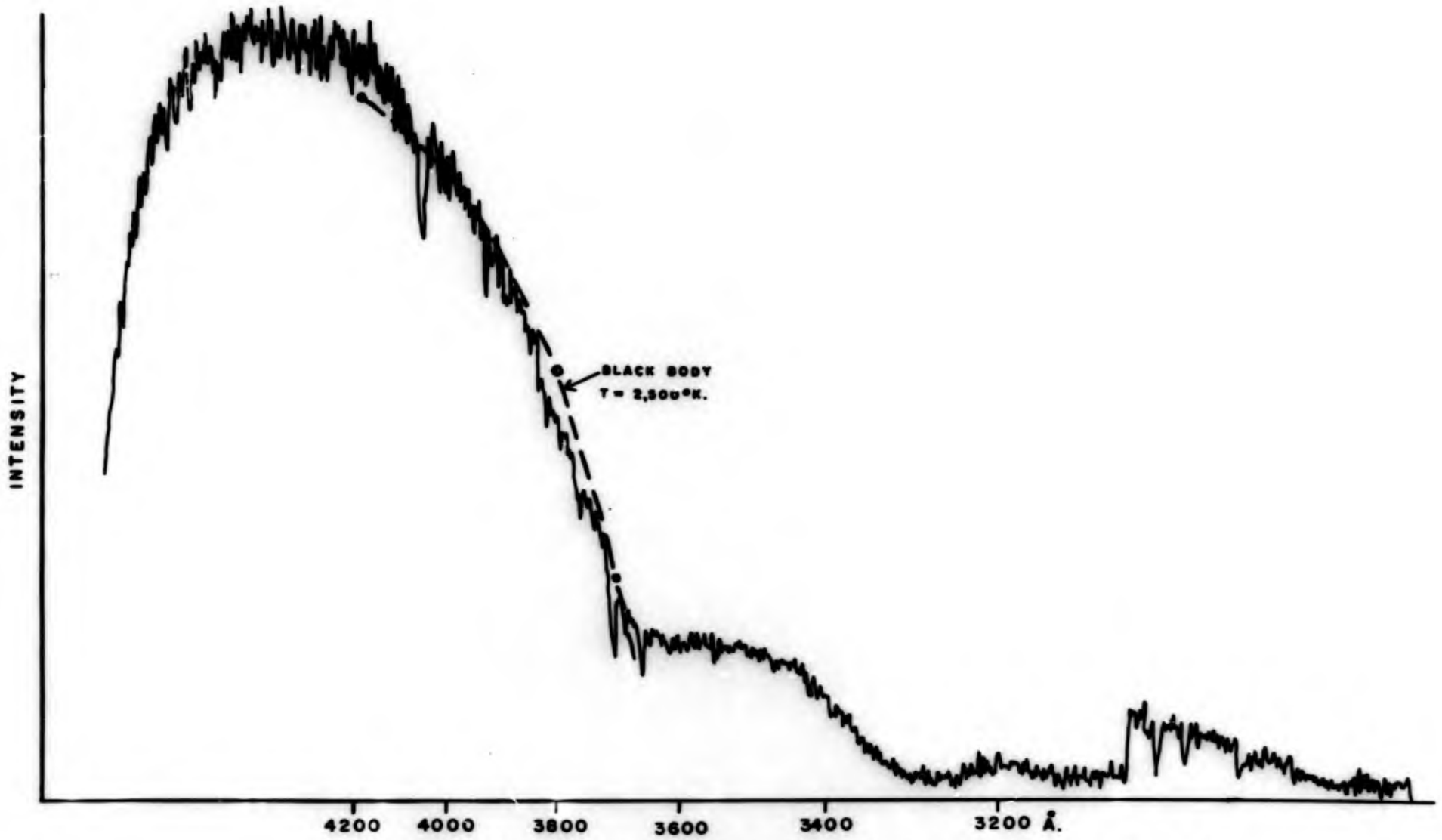

FIG. 7. TIME INTEGRATED SPECTRUM OF A GAS RUN [200 p.s.i., $2H_2 + O_2$].
(densitometer trace of plate in fig. 6 (a)).

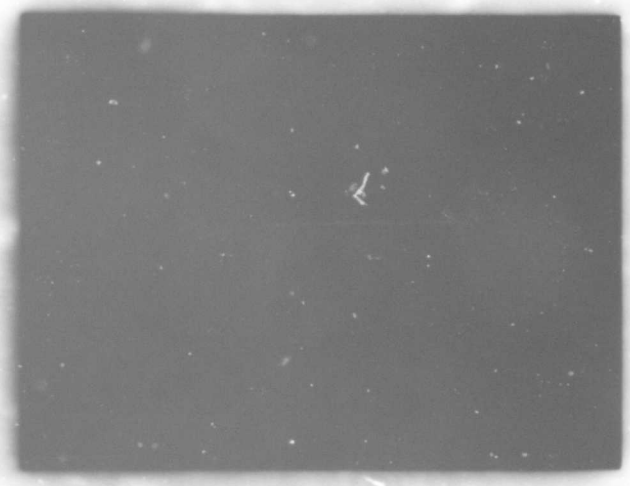

(a)

(b)

FIG. 8: TIME RESOLVED PHOTOMULTIPLIER RECORDS OF VISIBLE EMISSION FROM TWO GAS RUNS (200 p.s.i., $2H_2 + O_2$).

Horizontal scale: 10 μ sec./divn.
Vertical scale: Intensity (negative signal).

(The second peak in emission corresponds to the first implosion).

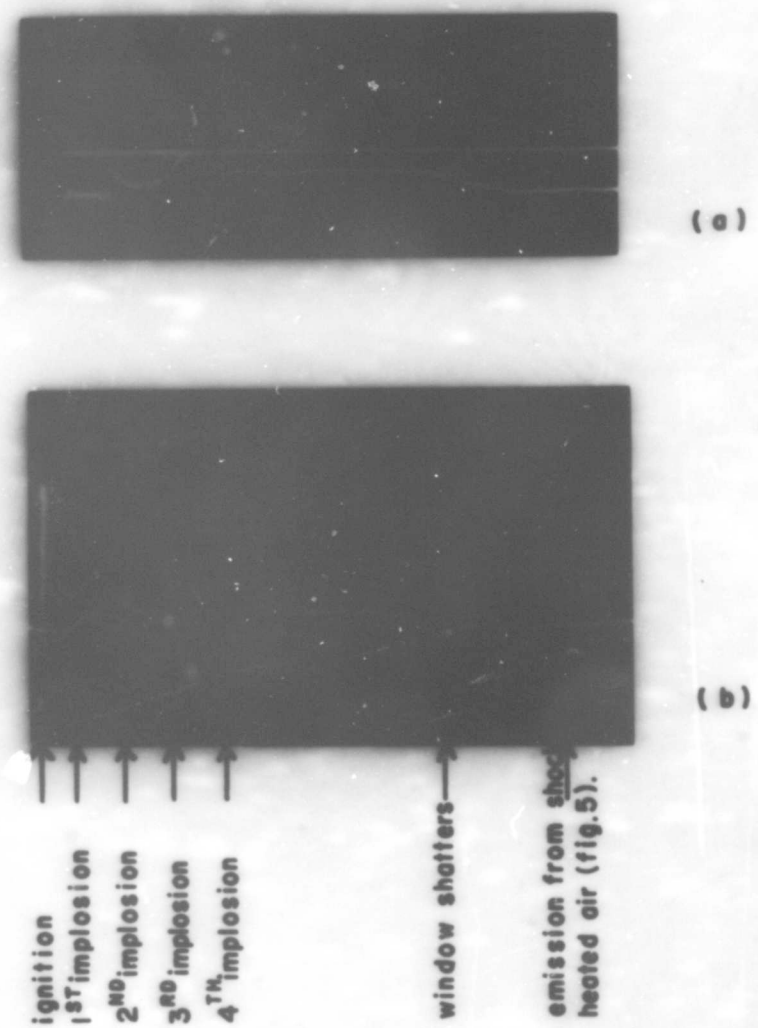

FIG. 9. TIME RESOLVED PHOTOELECTRIC RECORDINGS OF VISIBLE RADIATION FROM TWO GAS RUNS [200p.s.i., $2H_2+O_2$].

Showing multiple implosions and lack of repeatability of signal after first implosion.

(horizontal scale: 100μsec./divn.)

[The upper trace on (b) is a magnification of the 1ST — 2ND implosion region.]

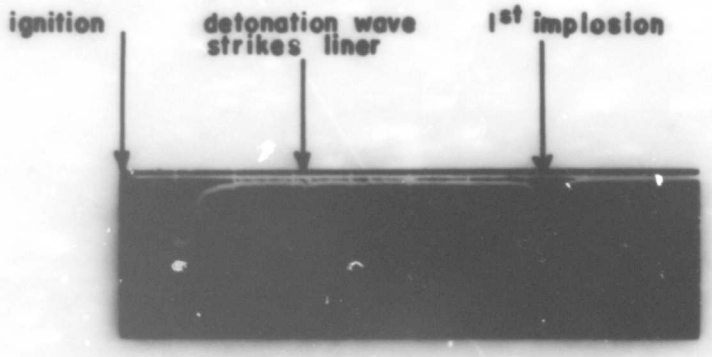

FIG. 10. PHOTOMULTIPLIER RECORD AT SHORT WAVELENGTH.
(100 Å bandwidth at $\lambda = 3656$ Å).
(horizontal scale: 10 μsec./divn.)

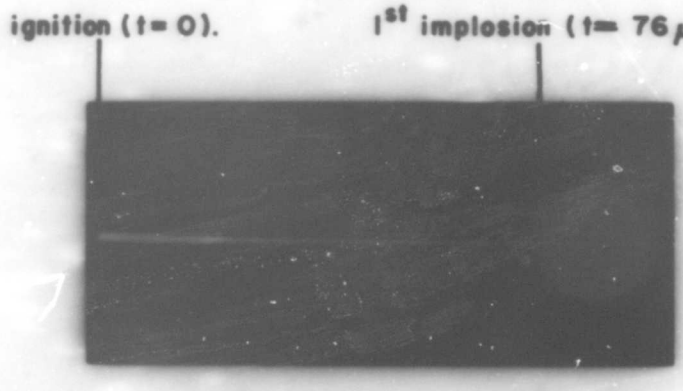

(a)

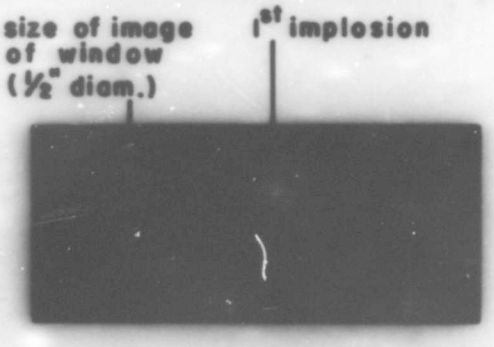

(b)

FIG. 11. FRAMING CAMERA PHOTOGRAPHS TAKEN THROUGH ½" DIAM. WINDOW AT ORIGIN OF THE UTIAS IMPLOSION DRIVEN HYPERVELOCITY LAUNCHER DURING A GAS RUN (200 p.s.i. $2H_2 + O_2$).

(a) Timing markers (10 μsec./divn.)

(b) Five frames at 2 μsec. intervals (exposure times 0.1 μsec.)

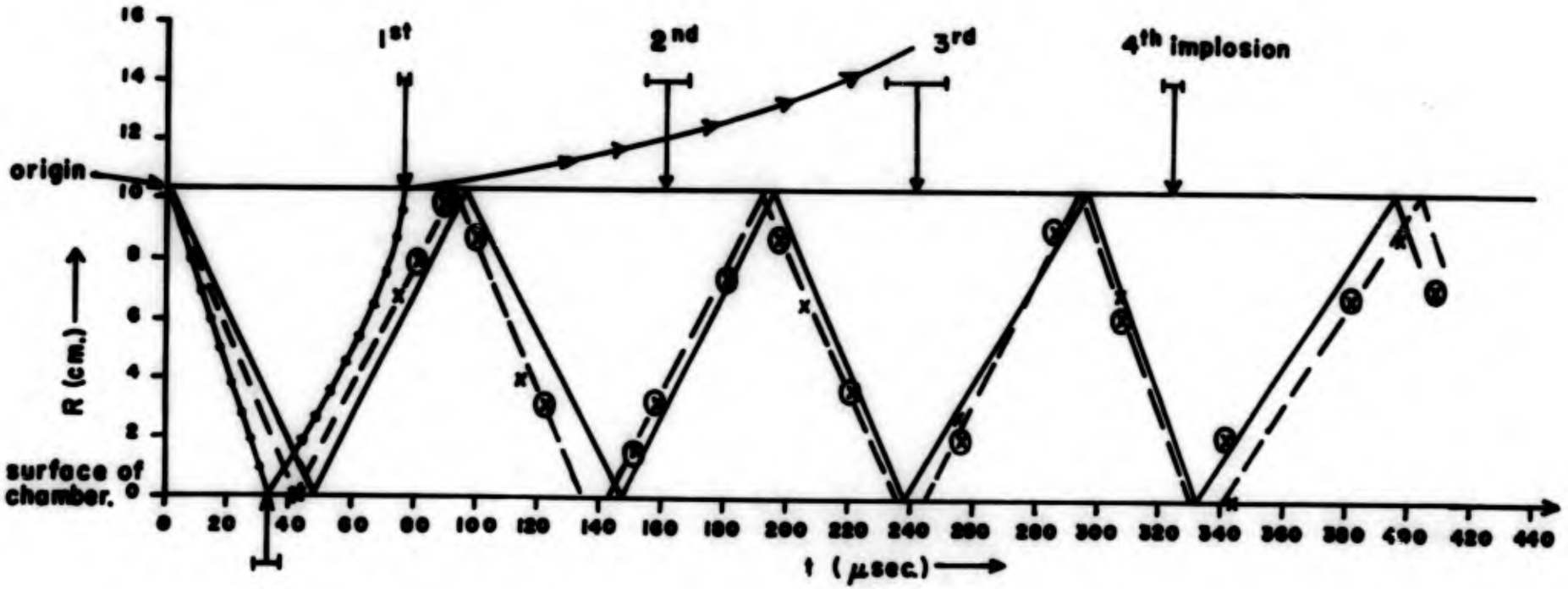

FIG. 12: WAVE AND PROJECTILE TRAJECTORIES FOR A GAS CASE (200p.s.i., $2H_2 + O_2$).

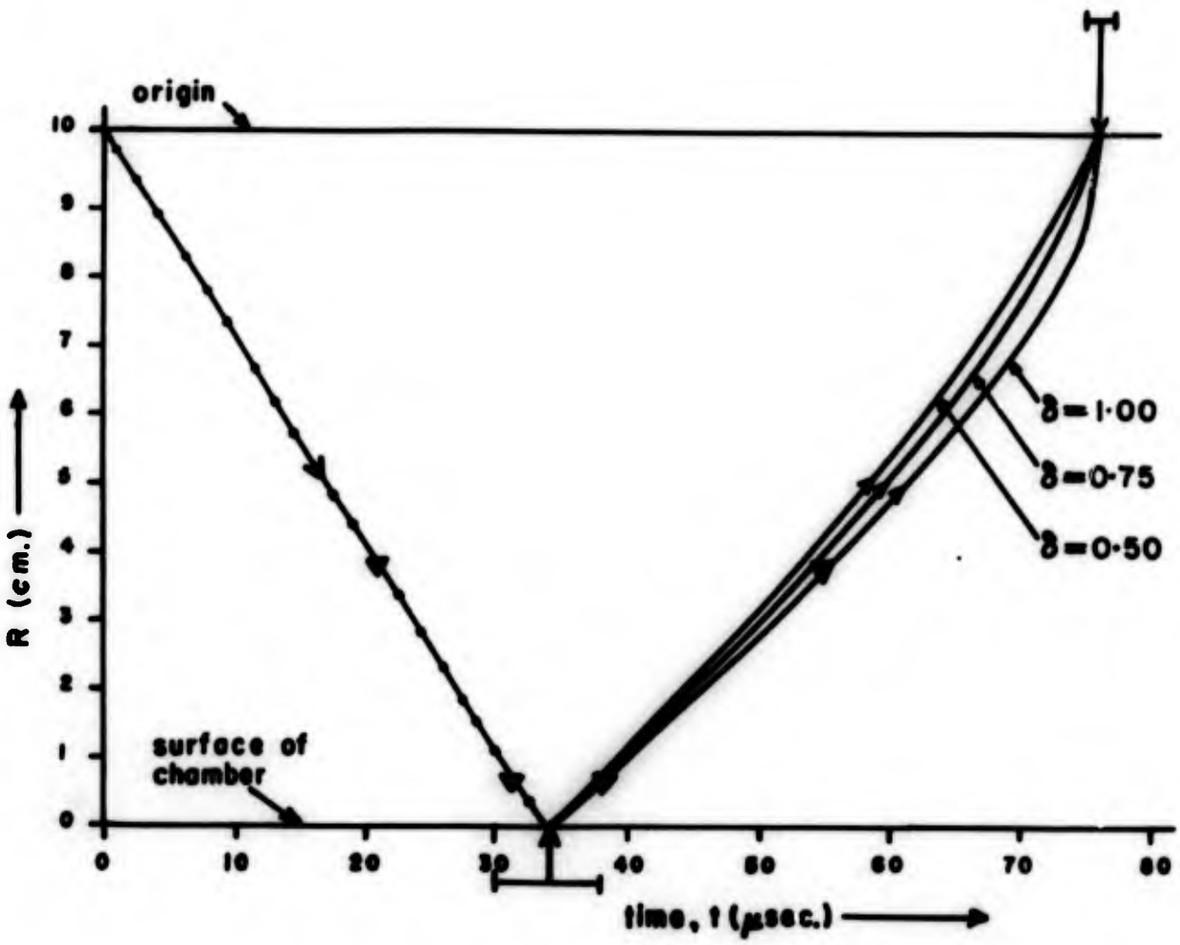

Measured points on trajectories

▼ Pressure probe (Watson, ref.2.)

↓ Spectroscopic (present work).

—•—•—•— Chapman–Jouguet detonation.

——— Classical implosion $R = \text{const.}\ t^{\frac{2}{2+\delta}}$.

FIG.13. COMPARISON OF MEASURED AND CLASSICAL IMPLOSION TRAJECTORIES (gas run, 200p.s.i., $2H_2 + O_2$).

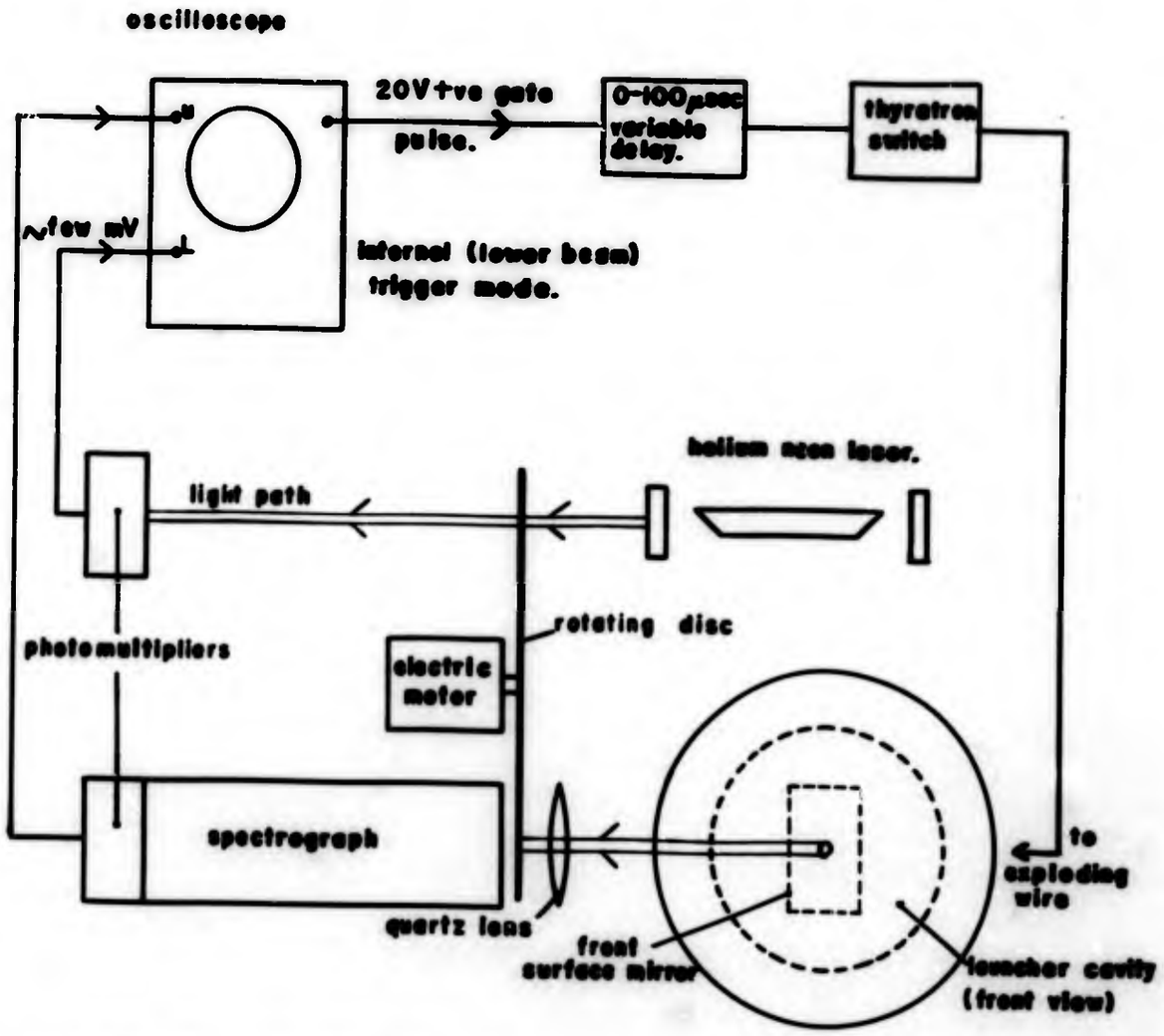

(a) GENERAL ARRANGEMENT.

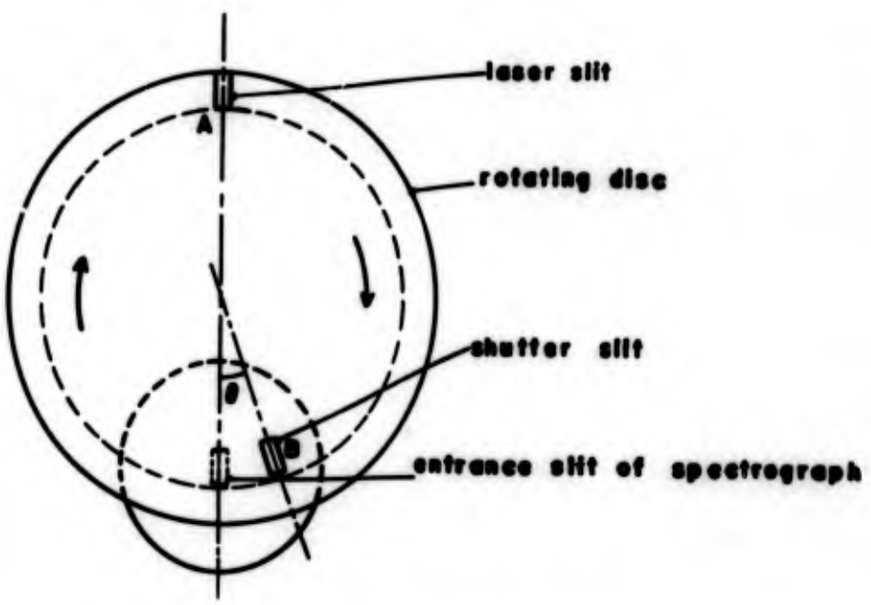

(b) FRONT VIEW OF SHUTTER

FIG. 14 SHUTTER OPERATION.

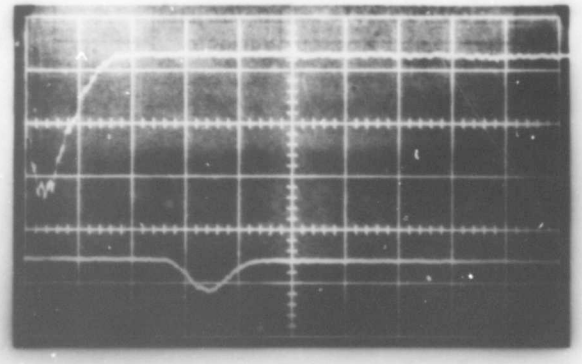

FIG.15: TRANSMISSION OF SHUTTER.

Upper beam: laser trigger pulse
Lower beam: shutter transmission
} 20μsec./divn.

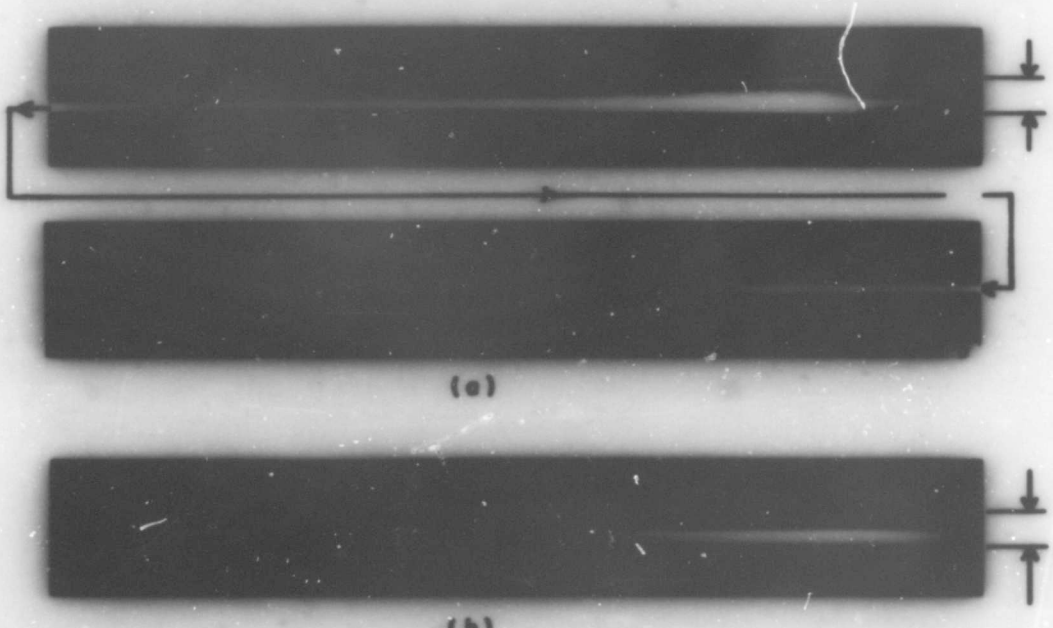

(a)

(b)

FIG.16: SHUTTERED SPECTRA OF (a) EXPLODING WIRE
(b) FIRST IMPLOSION

[gas run, 300p.s.i. $2H_2 + O_2$]

corresponds to the ½" window diameter.

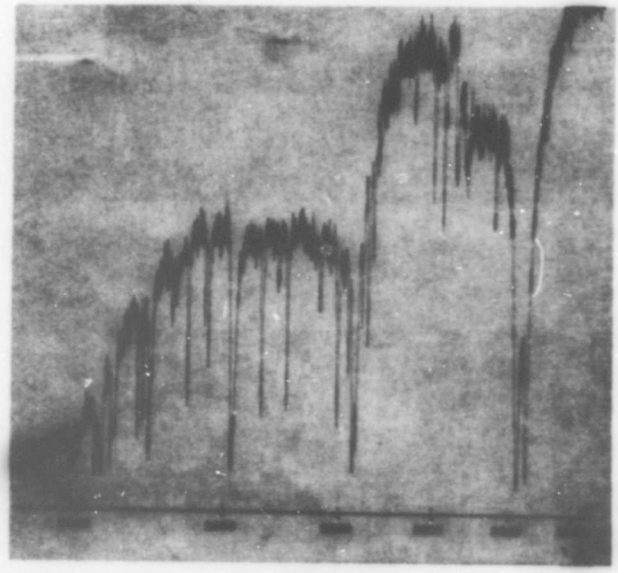

(a)

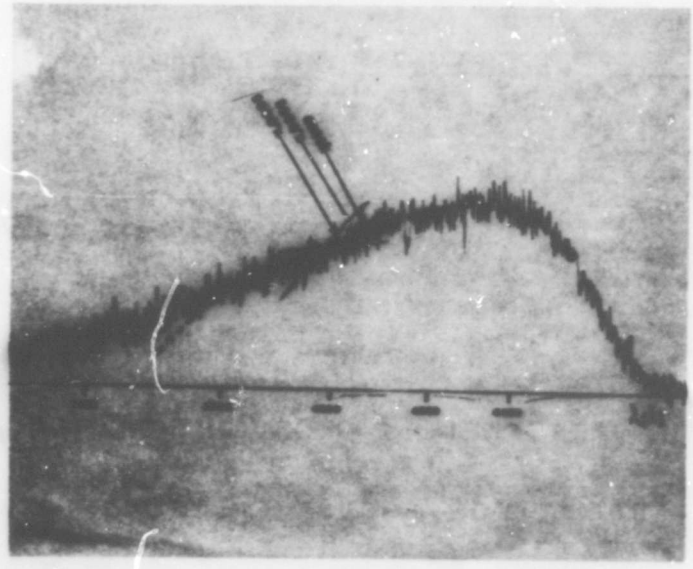

(b)

FIG. 17 · DENSITOMETER TRACES OF PORTIONS OF THE SPECTRA SHOWN IN FIGS. 16 (a) AND (b) RESPECTIVELY.

(a) exploding wire
(b) 1st implosion
] gas run, 300p.s.i. $2H_2 + O_2$.

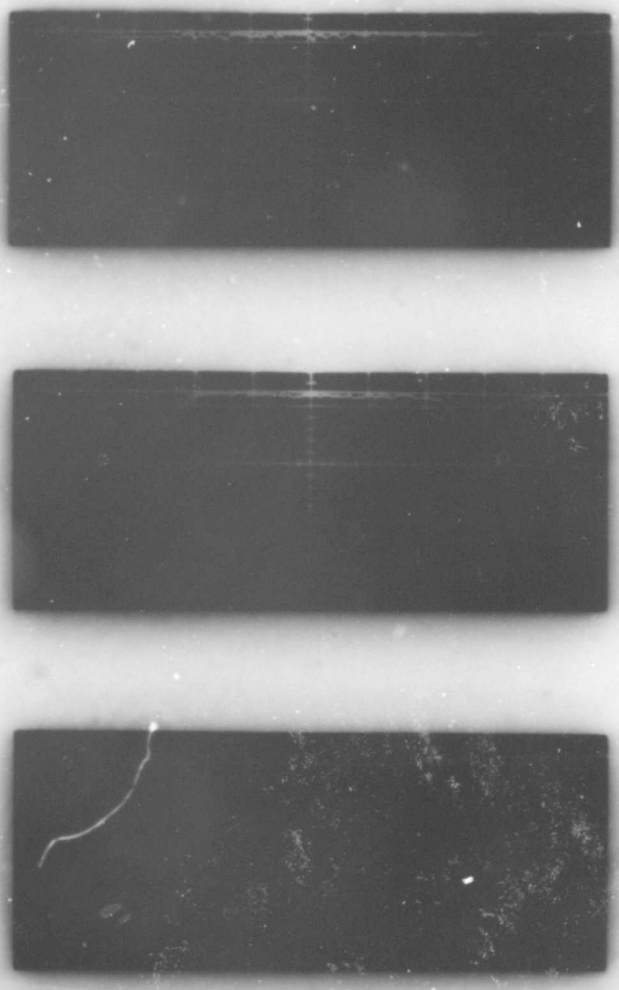

FIG. 18: TYPICAL 'STRASSHEIM' PHOTOMULTIPLIER RECORDS AT $\lambda = 3560$ Å. FOR 100 p.s.i. GAS RUNS WITH DIFFERENT HELIUM DILUTION.

horizontal scale: 10 μsec./divn.

(a) $2H_2 + O_2$.

(b) $2H_2 + O_2 + He$.

(c) $2H_2 + O_2 + 2He$.

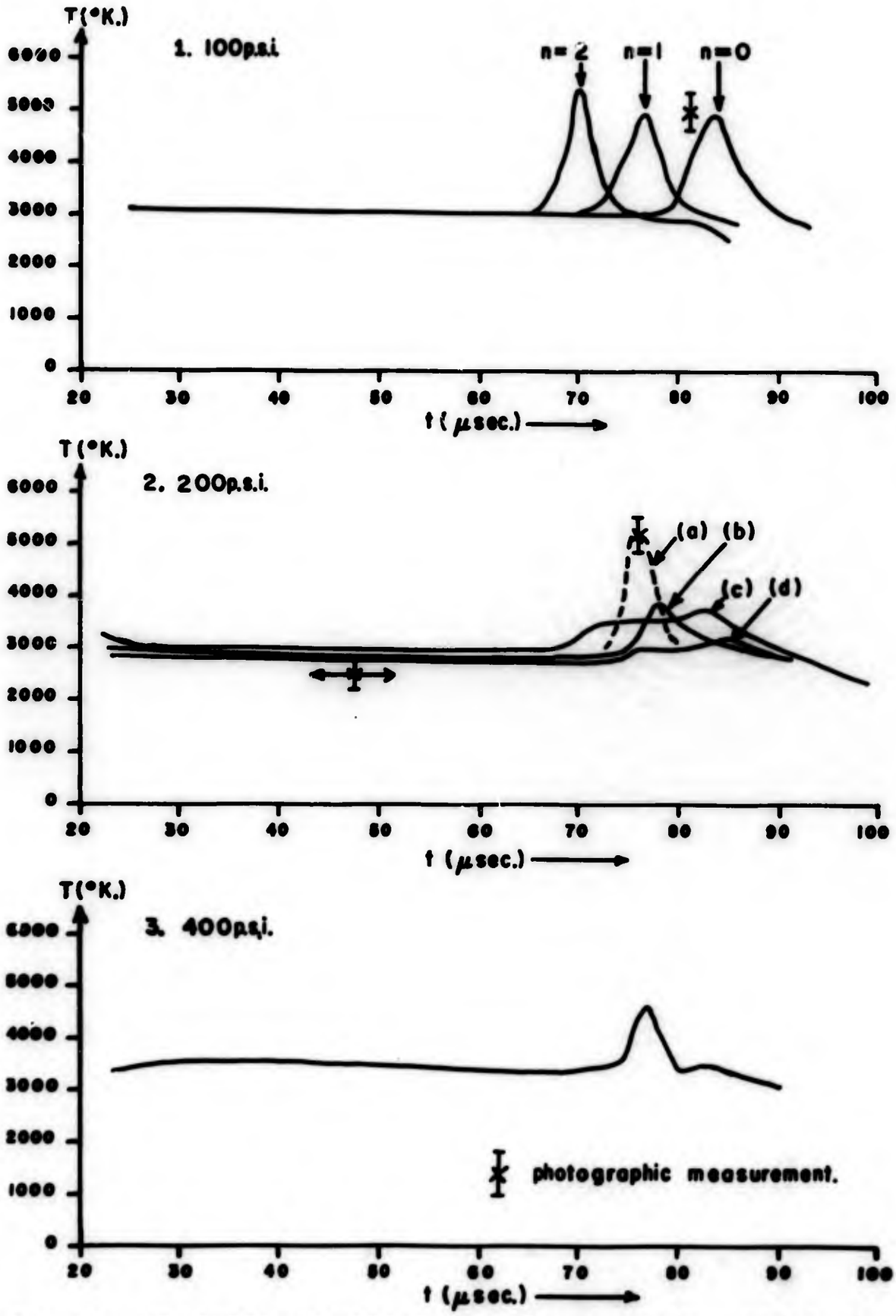

FIG. 19. MEASURED TEMPERATURE AT THE ORIGIN VERSUS TIME FOR DIFFERENT INITIAL PRESSURES AND DILUTIONS.

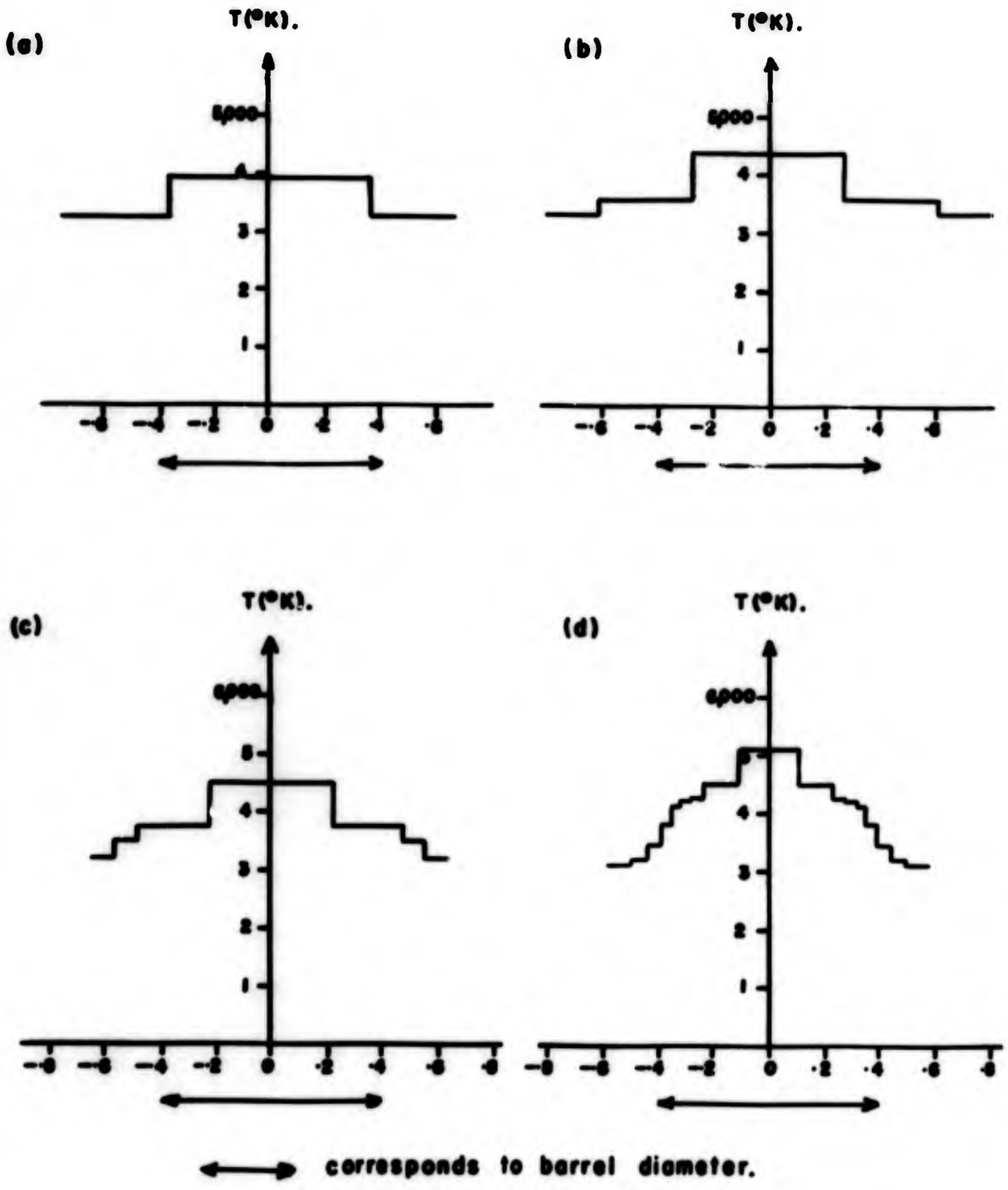

FIG. 20. CALCULATED TEMPERATURE DISTRIBUTIONS AT THE ORIGIN (1ST implosion) AS A FUNCTION OF THE NUMBER OF ZONES USED. (Calculations done by Eisenaar).

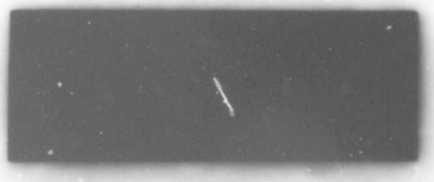

FIG. 21: FRAMING CAMERA SHOTS (corresponding to run 2d fig. 19).
(see fig. 11 for comparison).

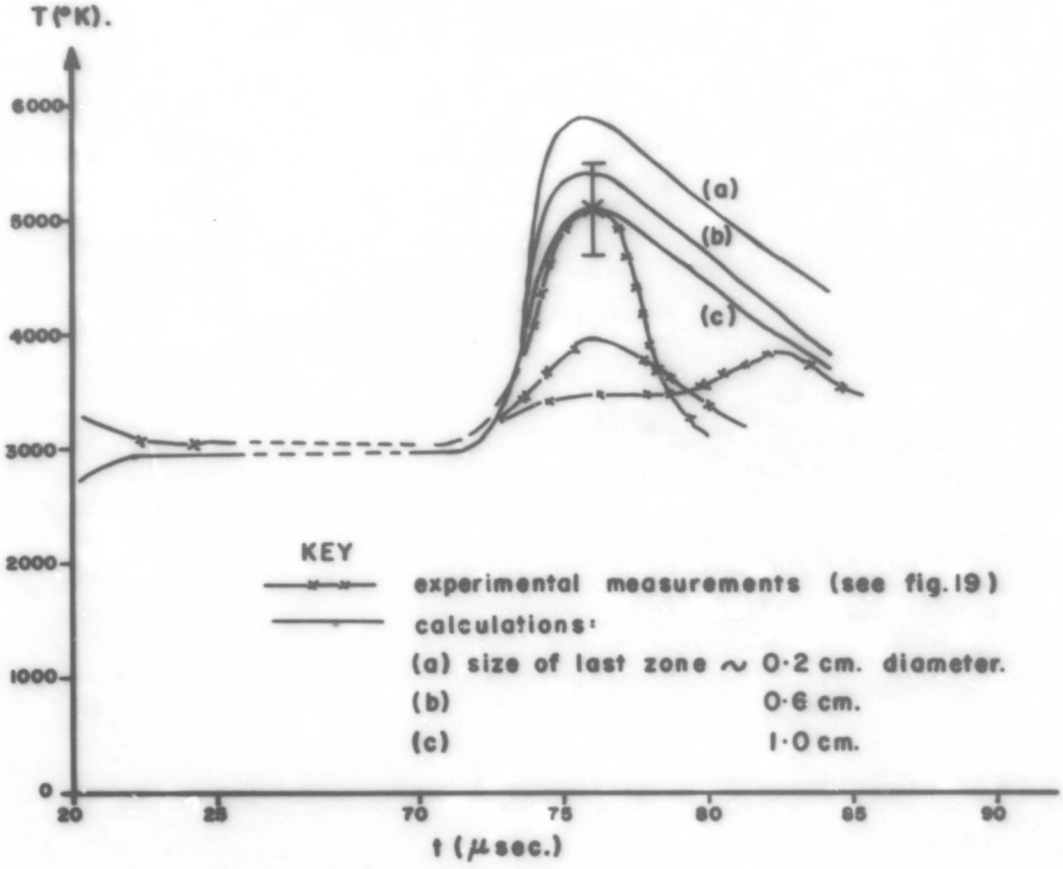

FIG. 22: COMPARISON OF MEASURED AND CALCULATED TEMPERATURES.
(200 p.s.i. gas run.)
(time axis shifted on calculated values — see 5·5)

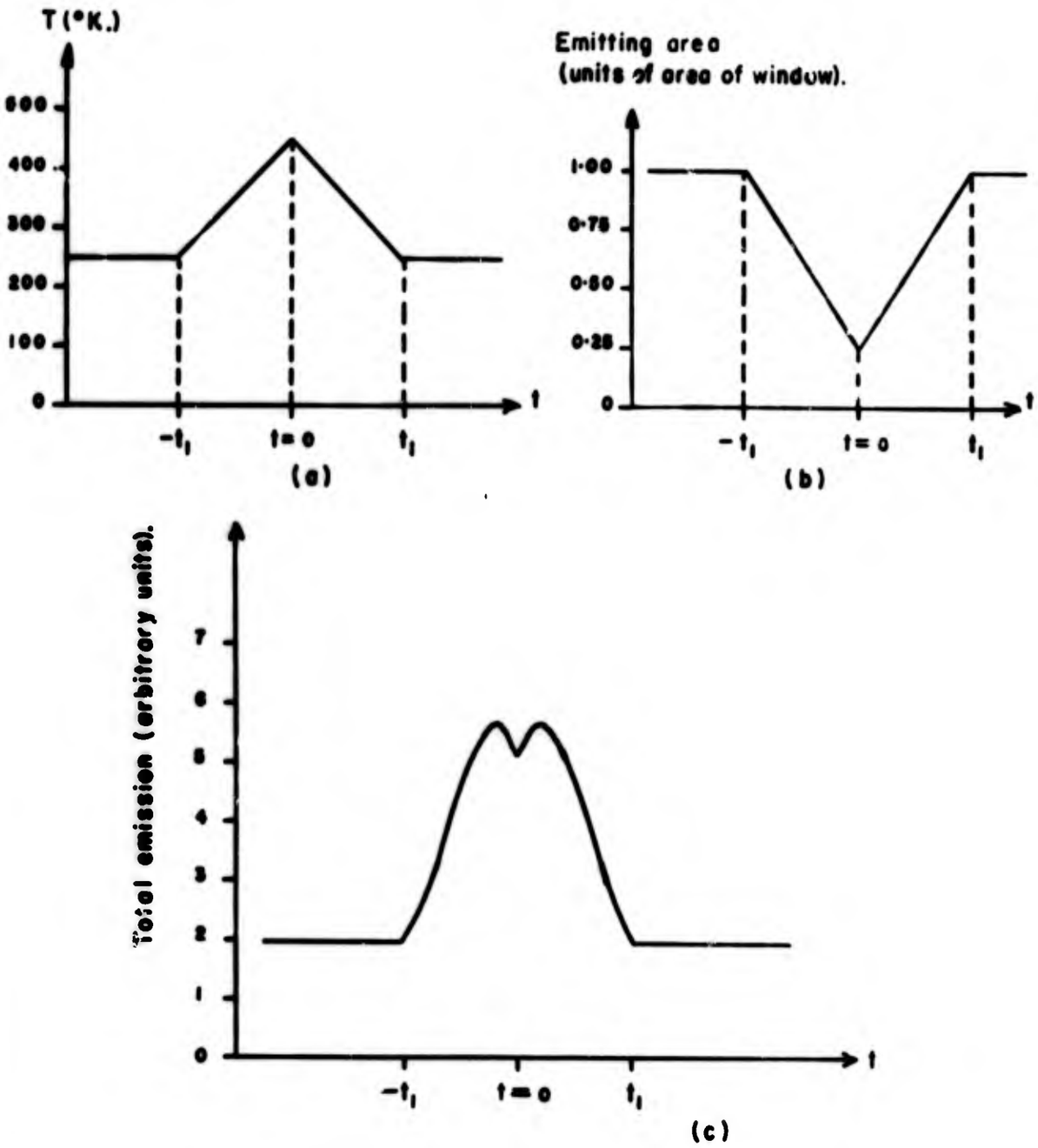

FIG. 23: CALCULATED TOTAL EMISSION (c), CORRESPONDING TO TEMPERATURE HISTORY (a), AND EMITTING AREA HISTORY (b). (t = 0 corresponds to the 1st implosion.) Compare with fig. 8(b).

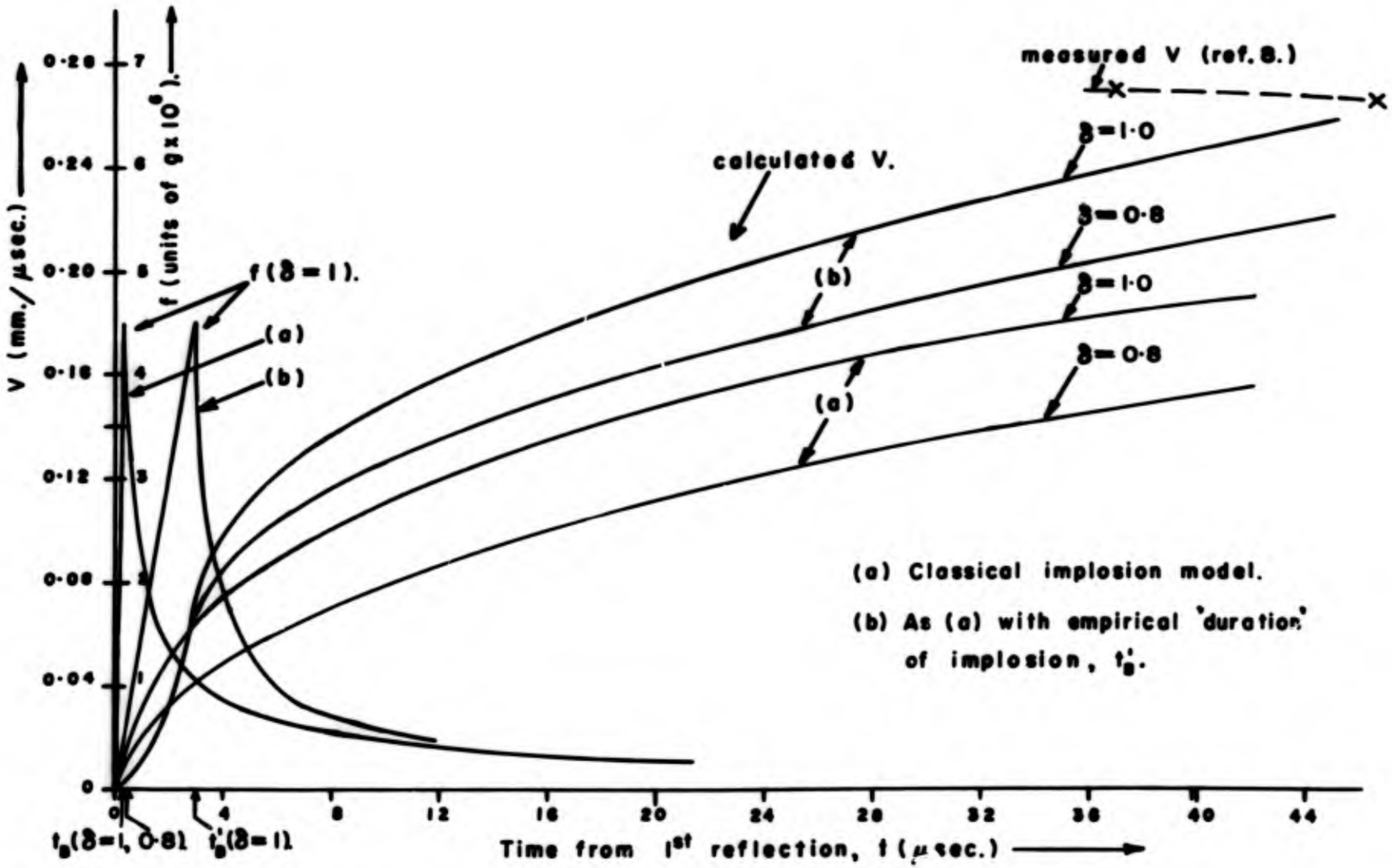

FIG. 24: CALCULATED ACCELERATION AND VELOCITY HISTORIES OF A 0·67 GRAM PROJECTILE DURING A 200 p.s.i. GAS RUN.

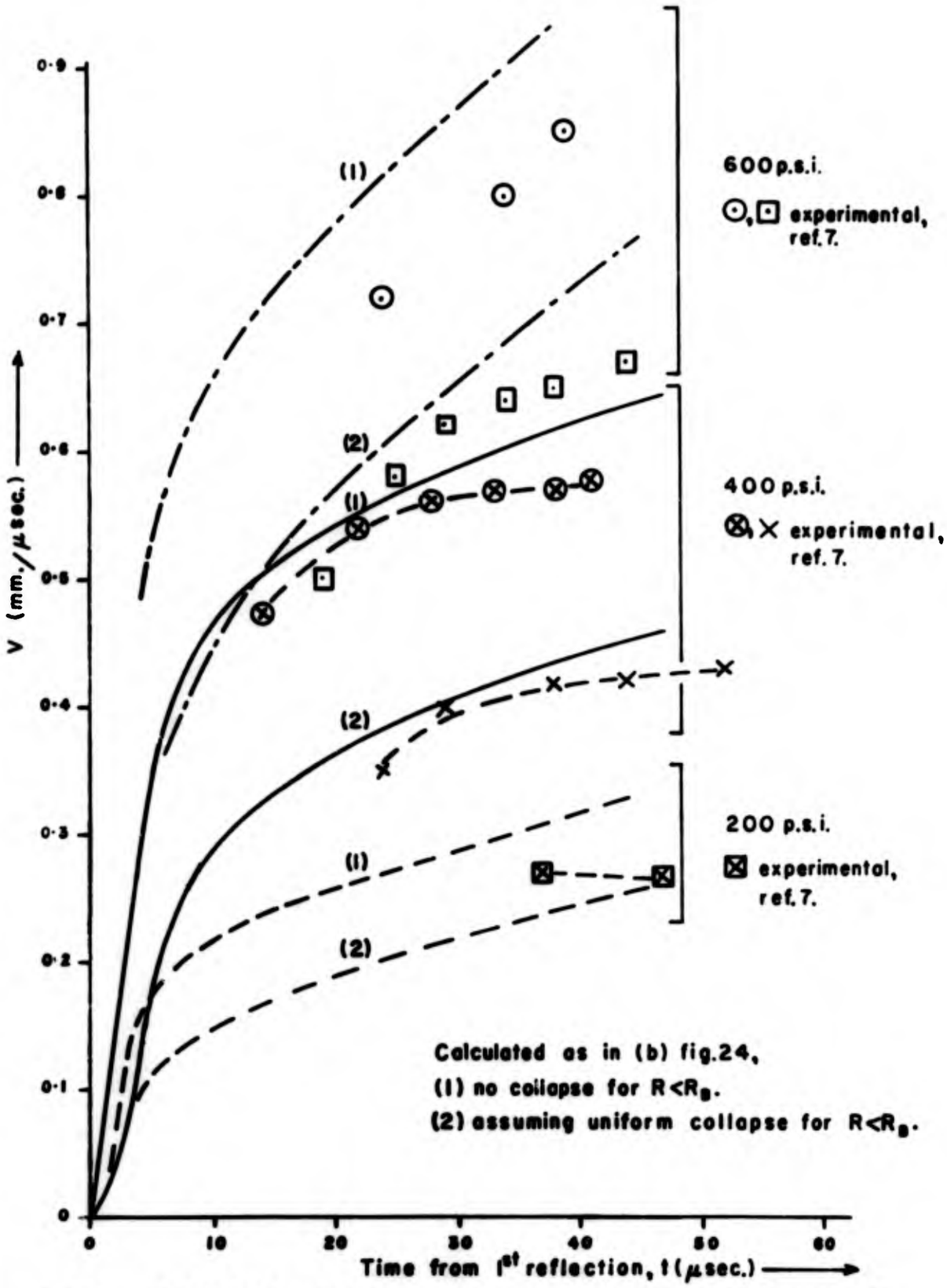

FIG. 25: CALCULATED VELOCITY HISTORY AS A FUNCTION OF INITIAL PRESSURE FOR A 0·67 GRAM PROJECTILE.